[American Journal of Science, Vol. 322, February, 2022, P. 164–189, DOI 10.2475/02.2022.03]

A NEOARCHEAN TO PALEOPROTEROZOIC MAGMATIC ARC IN THE TRANS-NORTH CHINA OROGEN: PETROLOGICAL AND GEOCHEMICAL CONSTRAINTS FROM THE TIANZHEN GNEISSES IN THE HUAI'AN COMPLEX

DINGYI ZHAO* and MIN SUN*,†

ABSTRACT. In the past two decades, extensive investigations have been carried out on the Trans-North China Orogen (TNCO), a Himalayan-type continental collisional belt along which the Eastern Block and the Western Block amalgamated to form the basement of the North China Craton. There are now coherent outlines of the timing and tectonic processes involved in the Paleoproterozoic amalgamation of the TNCO. However, pre-collisional tectonic setting and driving mechanism of the TNCO still remain controversial. To resolve these issues, we carried out field petrological and geochemical investigations on the Tianzhen gneisses from the Huai'an Complex in the TNCO. The Tianzhen gneisses consist predominantly of tonalitic-trondhjemitic-granodioritic (TTG) series, which can be further divided into low-Yb and high-Yb types. Our results indicate that although both low-Yb and high-Yb TTG series were formed in a magmatic arc environment, their petrogenetic origins were different. The Huai'an low-Yb TTG magma was derived from the partial melting of subducted oceanic crust consisting of eclogite or 30% garnet-bearing amphibolite under 15 to 20 kbar or even higher pressure, with garnet, amphibole, and rutile as residues. In contrast, the high-Yb TTG magma was derived from the partial melting of subducted oceanic slab consisting of garnet-free or 7% garnet amphibolite under 10 to 15 kbar, leaving residual garnet and amphibole. Both magmas then interacted with the overlying mantle wedge during ascent. Thus, it can be concluded that the Tianzhen TTG magmas were derived from the partial melting of subducted oceanic crust and interaction with mantle peridotite, supporting a magmatic arc setting for the Huai'an Complex during Neoarchean to Paleoproterozoic time. Associated with other analogous gneiss complexes in the TNCO, a long-lived Neoarchean to Paleoproterozoic magmatic arc system is established in the Trans-North China Orogen.

Key words: Huai'an Complex, Tonalitic-trondhjemitic-granodioritic (TTG), Trans-North China Orogen, magmatic arc, Neoarchean, Paleoproterozoic

INTRODUCTION

Considerable progress has been achieved in determining the geodynamic system and crustal evolution of the early earth, especially after numerous geochronological and isotopic studies determining continental growth and crust formation (Condie, 1998; Caro and others, 2005; Hawkesworth and others, 2009; Belousova and others, 2010; Rollinson, 2010; Dhuime and others, 2012; Condie and Kröner, 2013; Hawkesworth and others, 2019). The geodynamic model and driving mechanism for early Precambrian continental blocks to form cratons in the Archean remain controversial, with different workers advocating various processes including rifting, density-inversion, back-arc basin formation, arc-arc accretion, oceanic subduction, and arc- or continent-continent collision (Arndt, 1983; Hoffman, 1988; Kröner and Layer, 1992; Fukao and others, 2001; Zhao and others, 2002a; Romanowicz and Gung, 2002; Zhang and others, 2009; Santosh, 2010b). In addition, there are varying opinions as to when plate tectonics became operational on the earth (Condie and Kröner, 2008). As one of the oldest cratons in the world, the North China Craton (NCC) experienced

* Department of Earth Sciences, The University of Hong Kong, Pokfulam Road, Hong Kong, China
† Corresponding author: E-mail: minsun@hku.hk (M. Sun)

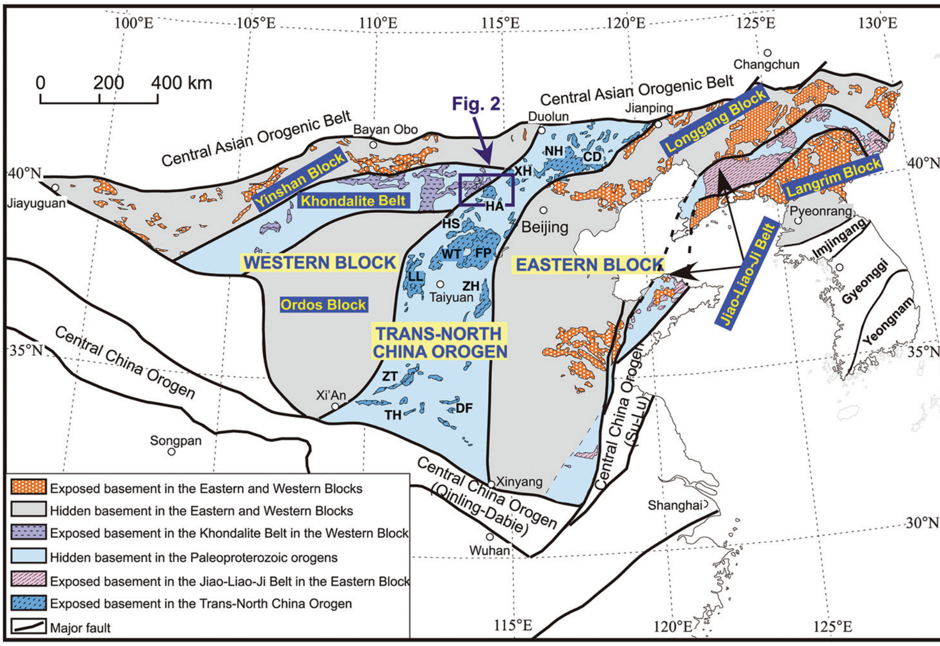

Fig. 1. Tectonic subdivision of the North China Craton, modified from Zhao and others (1998, 2001b, 2005). Abbreviations for metamorphic complexes: CD – Chengde; DF – Dengfeng; HA – Huai'an; LL – Lüliang; NH – Northern Hebei; TH – Taihua; WT – Wutai; XH – Xuanhua; ZH – Zanhuang; ZT – Zhongtiao; FP – Fuping; HS – Hengshan.

long-lasting evolution from ~3.8 to ~1.7 Ga (Liu and others, 1992; Wan and others, 2005; Zhai and Santosh, 2011; Zhao and Cawood, 2012; Zhai, 2014). The NCC has attracted much attention and three Paleoproterozoic collisional belts have been recognized, that are the Khondalite Belt in the west, the Trans-North China Orogen (TNCO) in the center, and the Jiao-Liao-Ji Belt in the east (fig. 1; Zhao and others, 2005). In the past two decades, researchers have carried out extensive geological investigations on the three belts. The Khondalite Belt has been considered as a continent-continent collisional belt, along which the Yinshan Block in the north and the Ordos Block in the south collided to form the Western Block at ~1.95 Ga (Zhao and others, 2003; Xia and others, 2006a, 2006b; Yin and others, 2009, 2011, 2014, 2015; Zhao, 2009; Zhou and others, 2010; Li and others, 2011b; Wang and others, 2011; Zhao and Zhai, 2013). The Jiao-Liao-Ji Belt is a rift-and-collisional belt, which experienced initial rifting of a continent and then opening of an ocean whose consumption and closure led to collision of two microcontinental blocks (that is, the Longgang and Langrim blocks) to form the Eastern Block at ~1.9 Ga (Luo and others, 2004, 2008; Li and others, 2005, 2011a, 2012; Li and Zhao, 2007, Zhou and others, 2008; Tam and others, 2011, 2012a, 2012b, 2012c). Finally, the Eastern and Western Blocks amalgamated along the TNCO to form the coherent basement of the NCC at about 1.85 Ga (Zhao and others, 2000, 2005, 2010, 2012; Guo and others, 2002, 2005; Wilde and others, 2002; Wilde and Zhao, 2005; Kröner and others, 2005b, 2005a, 2006; Zhang and others, 2006, 2007, 2012b; Li and others, 2010; Liu and others, 2012a, 2012b, 2012c, 2012e, 2013a).

However, much controversy has long surrounded the pre-collisional evolution of the TNCO. On the basis of geological and geochemical studies indicating that the basement rocks in the Trans-North China Orogen represent late Archean to

Paleoproterozoic magmatic arcs, a magmatic arc regime prior to continental collision was proposed to interpret formation and evolution of the Neoarchean basement rocks in the TNCO (Zhao and others, 2001b). On the contrary, other researchers argued that plate tectonics had not existed in the NCC until Proterozoic time. The evolution of NCC was thought to be controlled by frequent moderate-scale mantle plumes, accompanied by small-scale horizontal tectonic movements in the Archean (Geng and others, 2006; Zhai and Santosh, 2011; Zhai, 2012), based on voluminous tonalite-trondhjemite-granodiorite (TTG) rocks and associated komatiite-bearing magmatic suites in conjunction with Neoarchean greenstone belts.

TTGs are a composite rock suite that formed at a range of pressures from <10 to >25 kbar (Moyen, 2011). Sharing a common source, Archean granitic rocks from different geodynamics are broadly recognized as Archean TTGs, unlike modern granitoids consisting of a wider variety of rocks (Barbarin, 1999). Although it is commonly accepted that TTGs are sourced from hydrous basaltic rocks, one school of thought believed that TTGs were produced by slab melts in hot subduction zone (Martin, 1999; Foley and others, 2002; Martin and Moyen, 2002), whereas other researchers argued for a genetic mechanism of the partial melting of underplating hydrous basaltic source to the lower crust (Smithies and Champion, 2000; Condie, 2005). Corresponding to different advocated tectonic settings of the TNCO mentioned above, there are different interpretations for the origin of TTG rocks in the TNCO (Liu and others, 2012d; Zhai, 2012; Zhang and others, 2015; Shan and others, 2016; Wang and others, 2017).

The Huai'an Complex is located in the northern part of the TNCO (fig. 1) and contains well preserved high-grade gneisses, providing an ideal example to investigate crustal evolution of the TNCO. To resolve the above controversial issues, we conducted systematic petrological and whole-rock major and trace element analyses on the Tianzhen gneisses in the Huai'an Complex. Combined with previous studies on other areas of the TNCO, our results can place critical constraints on the pre-collisional setting and evolution of the TNCO, which further helps us determine early dynamic mechanisms on Earth.

GEOLOGICAL SETTING

The North China Craton (NCC), as one of the oldest continental blocks on Earth, underwent significant, multiphase crust formation, stabilization, and reworking (Liu and others, 1992; Song and others, 1996; Zhao and others, 2005; Zhai and others, 2011). The NCC is bounded by the Central Asian Orogenic Belt to the north and the Central China Orogen to the south (fig. 1). The craton consists mainly of Eoarchean to Paleoproterozoic basement overlain by Mesoproterozoic to Cenozoic unmetamorphosed cover (Zhao and others, 2001b). About 85% exposed basement in the NCC is composed of Neoarchean rocks, which are dominated by TTG gneisses with syntectonic granites and a variety of supracrustal rocks (Jahn and Zhang, 1984; Liu and others, 1985; Cui and others, 1991). The Eastern Block and the Western Block of the NCC amalgamated to form the coherent basement along the TNCO.

The TNCO, initially recognized by Zhao and others (1998), is a nearly south-north-trending belt with a length of about ~1200 km and a width of 100 to 300 km (fig. 1). The orogen consists of high-grade metamorphic gneiss complexes and low-grade or unmetamorphosed greenstone complexes (Zhao and others, 2001b; Zhao, 2014; Zhai, 2015). The high-grade gneiss complexes include the Huai'an, Taihua, Fuping, Hengshan, Xuanhua, and Chengde gneiss complexes, of which major lithologies are TTG gneisses commonly associated with high-pressure (HP) mafic and pelitic granulites with minor retrograde eclogites (Zhai and others, 1992, 1995; Guo and others, 1993, 2002). Through previous geochronological studies, Zhao (2014)

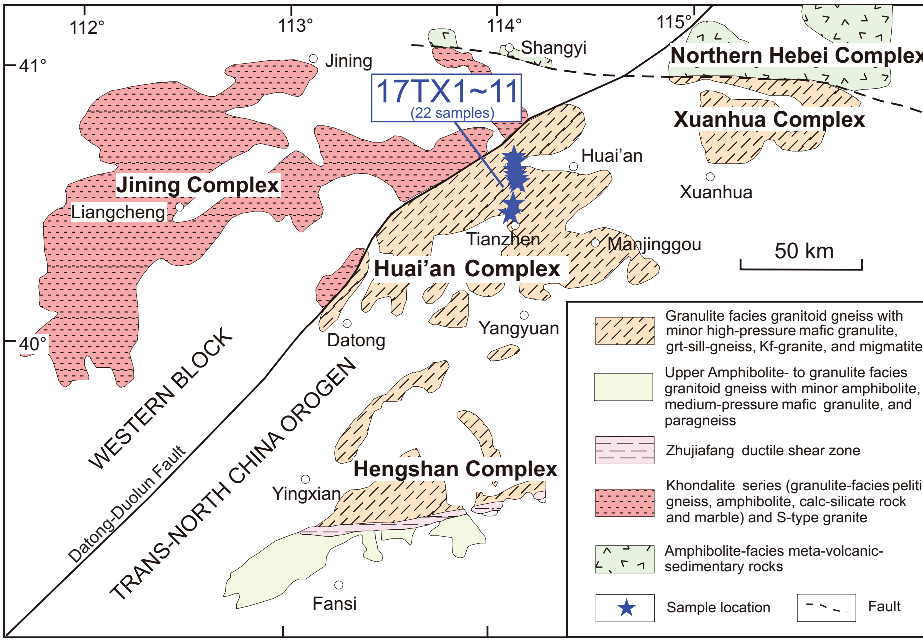

Fig. 2. Geological map of the Tianzhen area, modified from Zhao and others (2008a) and Liu and others (2012d).

systematically summarized the major lithologies of the TNCO and their ages, including: (i) minor 2.8 to 2.7 Ga grey gneisses and xenocrystic zircons that are interpreted as the remnants of the pre-orogenic old continental basement; (ii) 2.55 to 2.52 Ga granitoid plutons in the low- to medium-grade granite-greenstone terranes; (iii) 2.53 to 2.52 Ga greenstone assemblages; (iv) 2.52 to 2.475 Ga high-grade TTG gneisses; (v) 2.36 to 2.05 Ga Paleoproterozoic granitoid gneisses; (vi) Paleoproterozoic sedimentary-volcanic successions; (vii) 2.19 to 1.92 Ga mafic dikes that were metamorphosed to amphibolites and medium- to high-pressure mafic granulites; and (viii) 1.80 to 1.75 Ga post-orogenic or anorogenic mafic dikes. These lithologies robustly support the TNCO as a continent-continent collisional belt (Zhao, 2001, 2014; Zhao and others, 2005).

The Huai'an Complex is located in the northern part of the TNCO, adjacent to the northern part of the Hengshan Complex and the southwestern part of the Xuanhua Complex (fig. 2). The Huai'an Complex is separated from the easternmost part of the Paleoproterozoic Khondalite Belt (that is the Jining Complex) by a detachment fault (that is, the Datong-Duolun fault), accommodating extension after crustal thickening (Zhao and others, 1998, 2001b, 2008a; Guo and others, 2002, 2005; Zhang and others, 2006). The Khondalite belt is composed of ~60% "Khondalite Series", a supracrustal suite dominated by metapelites, calc-silicate rocks, and marbles, and ~40% S-type granites (Lu and Jin, 1993; Lu and others, 1996). The Huai'an rocks consist predominantly of TTG gneisses with minor gabbroic, dioritic, and granitic gneisses, most of which experienced upper amphibolite- to granulite-facies metamorphism and polyphase deformation (Wang and others, 2010). In the field, TTG gneisses show prominent gneissosity (fig. 3A and B) and are in contact with dioritic gneisses (fig. 3A). In addition, a small number of meta-supracrustal rocks (called "khondalite series" rocks in the Chinese literature) and gneissic granitoids (2.3–2.0 Ga) are exposed in the Huai'an Complex (Zhao and others, 2005, 2008a). U-Pb

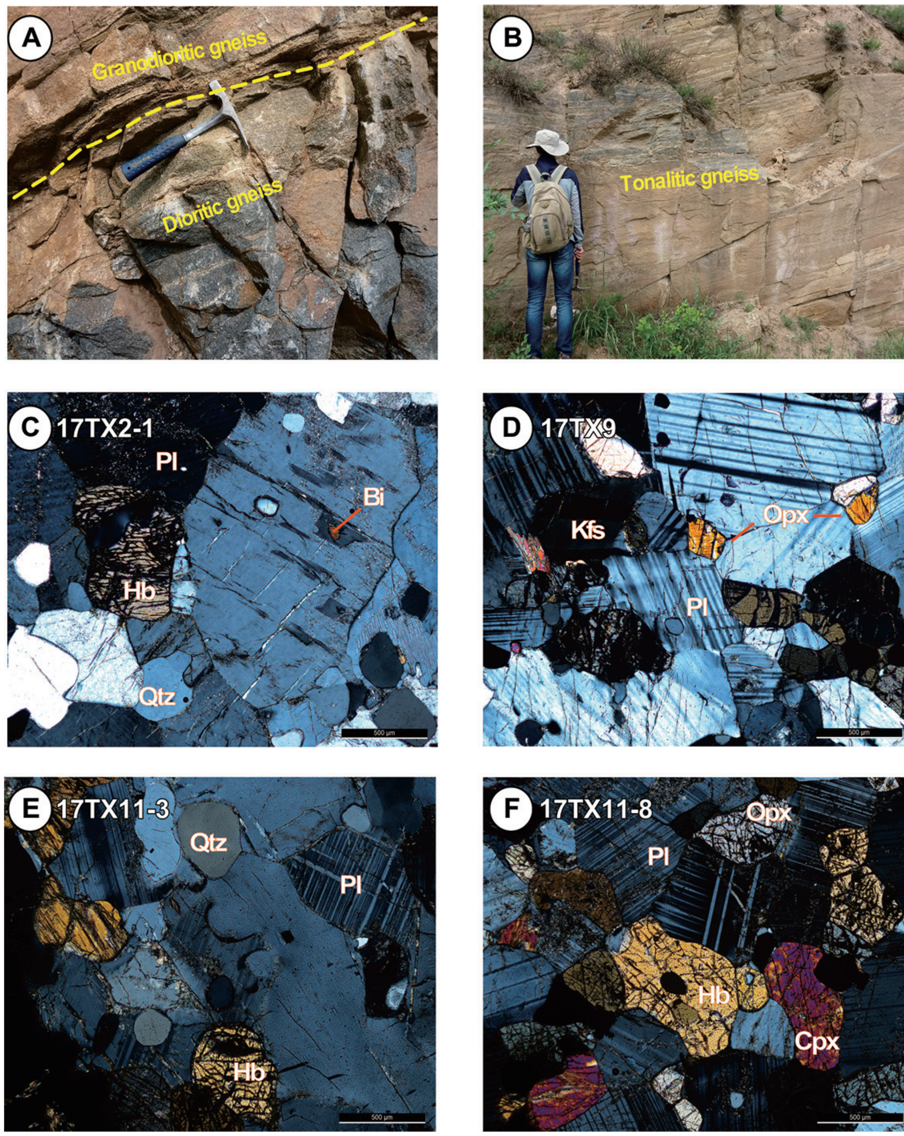

Fig. 3. Field photographs and photomicrographs (crossed polars) of representative samples from the Tianzhen area. (A) Granodioritic gneisses contacting with dioritic gneisses (Sample 17TX3-2 and Sample 17TX3-1); (B) Tonalitic gneisses (Sample 17TX1); (C) Trondhjemitic gneiss (Sample 17TX2-1); (D) Dioritic gneiss (Sample 17TX9); (E) Granitic gneiss (Sample 17TX11-3); (F) Gabbroic gneiss (Sample 17TX11-8). Mineral abbreviations are as follows: Hb – hornblende, Bi – biotite, Pl – plagioclase, Qtz – quartz, Kfs – K-feldspar, Opx – Orthopyroxene, Cpx – Clinopyroxene.

dating and Nd-Hf isotopic analyses revealed that the protolith of the Huai'an gneisses formed at about 2.5 to 2.4 Ga (Zhao and others, 2008a; Liu and others, 2009b; Su and others, 2014). The dating results were also confirmed by previous work on samples from the same field work as this study, including some of the samples in this study (Zhao and others, 2020). 1.9 to 1.8 Ga HP mafic granulites occur as enclaves or small sheets within the Huai'an gneisses (Zhai and others, 1993; Zhang and others, 1994; Dirks and others, 1997; Li and others, 1998; Wu and others, 2016). Similar to those in other complexes of the TNCO, HP mafic granulites in the Huai'an Complex record clockwise P–T paths defined by four metamorphic stages, that is: prograde metamorphism (M1), peak metamorphism (M2), near-isothermal decompression (M3), and cooling (M4), which is in accordance with tectonic processes involving the collision between the Western and Eastern Blocks along the TNCO at ~1.8 Ga (Guo and others, 2002; Zhang and others, 2006; Zhao and others, 2008a; Wu and others, 2019).

SAMPLING, PETROGRAPHY, AND ANALYTICAL TECHNIQUES

In this study, we collected twenty-two representative gneissic samples of TTG from the Tianzhen area of the Huai'an Complex (fig. 2), of which nine samples are TTG gneisses, ten samples are dioritic gneisses, two samples are gabbroic gneisses, and one sample is granitic gneiss (fig. 3). The nine TTG gneissic samples comprise six tonalitic gneisses, two granodioritic gneisses, and one trondhjemitic gneiss with mineral assemblages of plagioclase (50–55%), quartz (20–25%), K-feldspar (<5%), biotite (<5%), amphibole (<5%), and hypersthene (<5%) (fig. 3C). The dioritic gneisses consist of plagioclase (50–55%), quartz (10–15%), hypersthene (10–15%), diopside (<5%), K-feldspar (<5%), and biotite (<5%) (fig. 3D). The gabbroic gneisses are composed of plagioclase (<50%), diopside (<20%), hypersthene (5–10%), quartz (<5%), amphibole (<5%), K-feldspar (<5%), and biotite (<5%) (fig. 3F). The granitic gneiss is dominated by plagioclase (30–38%), K-feldspar (20–25%), and quartz (<25%), with minor amphibole (<5%), biotite (<5%), and hypersthene (<2%) (fig. 3E). Magnetite, ilmenite, zircon, and apatite are common accessory minerals in the gneisses. The mineral assemblages preserved in the TTG and dioritic gneissic samples indicate predominant amphibolite- to granulite-facies metamorphism. Most gneisses display microscopic granoblastic and triple junction textures with a gneissic structure defined by oriented biotite and a lineation defined by oriented hornblende.

Whole-rock major and trace element analyses were conducted on all the samples, which were initially trimmed to remove weathered surfaces and then the fresh portion was chipped and powdered in an agate mill to about 200 mesh. Whole-rock major element compositions were analyzed using an X-ray fluorescence spectrometer (XRF) (PANalytical-AxiosmAX, Netherlands) at FocuMS Technology Co., Ltd., Nanjing, China. About 0.6 g of powder was fused with 6 g latent solvent ($Li_2B_4O_7$ + $LiBO_2$ + LiBr), then placed into a ceramic crucible, and fused again at 1100 °C in a Pt-Au crucible for 30 mins. The resultant melt was poured into pre-heated pellet and prepared for major element analysis. The international reference standard BHVO-2 and national standards GBW07315 and GBW07316 were analyzed for quality control. The XRF analytical precision of 2% meets the Chinese National Standard GB/T14506.28-2010 (National Standard of P.R. China) (2011).

Whole-rock trace element analysis was carried out by Inductively Coupled Plasma Mass Spectrometry (ICP-MS) at FocuMS Technology Co., Ltd., Nanjing, China. About 40 mg of powder was mixed with 0.5 ml HNO_3 and 1.0 ml HF in high-pressure PTFE bombs. These bombs were steel-jacketed and placed in an oven at 195 °C for 48 hours for mafic samples and 72 hours for felsic samples. Rock digestion diluent was nebulized into an Agilent Technologies 7700x quadrupole ICP-MS (Hachioji, Tokyo, Japan) to obtain trace element results. Geochemical reference materials of USGS andesite (AGV-2), diabase (W-2), and slate (OU-6) were analyzed for quality control. Measured values of these reference materials were compared with preferred values in GeoReM database (Jochum and Nohl, 2008; http://georem.mpch-mainz.gwdg.de). Deviation was better than ± 10% for elements exceeded 10 ppm and better than ± 5% for elements exceeded 50 ppm.

ANALYTICAL RESULTS

The whole-rock major and trace element compositions of the twenty-two samples from the Tianzhen area are listed in table 1. According to the Yb composition, the gneissic samples in this study can be further divided into a low-Yb subgroup (Yb contents of 0.05–0.47 ppm with an average of 0.26 ppm) and a high-Yb subgroup (Yb contents of 0.75–3.44 ppm with an average of 1.67 ppm). The two groups show different geochemical characters, especially with respect to MgO, heavy rare earth elements (HREE) composition, and Eu anomalies, as discussed below. In addition, the low-Yb subgroup has lower contents of mafic minerals and is comparatively more leucocratic than the high-Yb subgroup.

Major Elements

The low-Yb group is composed of five TTG gneisses, two dioritic gneisses, and one granitic gneiss. Five TTG gneisses have SiO_2 contents of 67.94 to 76.86 wt.%, CaO contents of 2.89 to 4.35 wt.%, Na_2O/K_2O ratios of 1.20 to 3.79, and Mg# values (100 $Mg/(Mg + Fe^{2+})$) of 27 to 52 (average of 45), whereas the two dioritic gneisses are characterized by slightly lower SiO_2 contents of 54.38 and 60.31 wt.%, higher CaO contents, higher Na_2O/K_2O ratios of 3.49 and 4.22, and higher Mg# values of 54 and 57. The granitic gneiss has SiO_2 of 71.53 wt.%, CaO of 2.07 wt.%, Na_2O/K_2O of 0.68, and an Mg# value of 43 (table 1).

The high-Yb group consists of four TTG gneisses, eight dioritic gneisses, and two gabbroic gneisses. The TTG gneisses have SiO_2 contents of 62.70 to 66.86 wt.%, CaO contents of 3.88 to 5.29 wt.%, Na_2O/K_2O ratios of 1.40 to 2.55, and Mg# values of 50 to 55. Comparatively, the dioritic gneisses are characterized by slightly lower SiO_2 contents of 51.41 to 60.94 wt.%, higher CaO contents, higher Na_2O/K_2O ratios of 1.31 to 5.72, and higher Mg# values of 40 to 56 (average of 48) than those of the TTG gneisses. Two gabbroic gneisses have SiO_2 of 50.00 and 49.53 wt.%, CaO of 10.32 and 10.48 wt.%, Na_2O/K_2O of 4.26 and 2.69, and Mg# values of 46 and 51 (table 1).

As shown in the Ab-An-Or diagram (fig. 4A), six TTG gneissic samples plot in the tonalite field, two in the granodiorite field, and the other one plots as trondhjemite. There is no distinction between the low-Yb and high-Yb samples, and most of them are classified as calc-alkaline in the K_2O versus SiO_2 diagram (fig. 4B). However, differences exist between the low-Yb and high-Yb groups. For example, the low-Yb samples mainly exhibit peraluminous characteristics, whereas most high-Yb samples are metaluminous with much lower A/CNK ($Al_2O_3/(CaO+Na_2O+K_2O)$) ratios (fig. 4C). In addition, marked differences are illustrated in the MgO versus SiO_2 diagram (fig. 4D), in which most of the low-Yb gneisses show similar characters with high-silica adakite with MgO compositions lower than 1.44 wt.%, except for two dioritic gneisses. The high-Yb gneisses plot in the field of both low-silica and high-silica adakite with MgO composition higher than 2.00 wt.%, except for one dioritic gneiss.

Trace Elements

The low-Yb gneisses.—In the chondrite-normalized REE diagram, the low-Yb gneisses are characterized by fractionated REE patterns with strongly depleted HREE contents and positive Eu anomalies (fig. 5A). Among the low-Yb gneissic samples, the TTG gneisses display total HREE and rare earth elements (REE) contents of 0.64 to 2.50 and 24.68 to 68.73 ppm, respectively, with δEu (Eu/Eu*) ratios of 2.32 to 3.23 and $(La/Yb)_N$ values of 30.52 to 96.88, while two dioritic gneisses exhibit HREE and REE contents of 3.38 to 3.53 and 38.30 to 39.07 ppm with slightly lower δEu (Eu/Eu*) ratios and lower $(La/Yb)_N$ values. The granitic gneiss has HREE and REE contents of 3.30 and 109.24 ppm, with the δEu (Eu/Eu*) of 1.57 and $(La/Yb)_N$ value of

TABLE 1

Major- (wt.%) and trace-element (ppm) compositions of the Tianzhen gneisses

Sample No.	17TX1	17TX2-1	17TX2-2	17TX3-3	17TX11-1	17TX11-4	17TX11-7	17TX11-3	17TX3-2	17TX4-1
Low-Yb: TTG gneisses						Dioritic gneisses		Granitic gneiss	*High-Yb:* TTG gneisses	
SiO_2	76.86	70.68	69.01	70.53	67.94	54.38	60.31	71.53	66.86	62.70
TiO_2	0.03	0.22	0.31	0.22	0.18	0.24	0.11	0.19	0.42	0.54
Al_2O_3	13.09	16.49	16.78	14.77	17.34	24.44	21.51	14.84	14.83	16.21
Fe_2O_3	0.52	1.31	2.16	2.62	1.75	2.43	2.06	1.38	4.76	4.72
MnO	0.00	0.01	0.02	0.04	0.02	0.03	0.04	0.01	0.06	0.07
MgO	0.09	0.54	1.19	1.19	0.97	1.44	1.38	0.52	2.38	2.95
CaO	2.94	2.89	4.19	3.00	4.35	9.13	7.18	2.07	3.88	5.01
Na_2O	3.71	5.10	4.22	3.39	4.40	5.00	5.03	3.25	3.34	4.05
K_2O	0.98	1.74	1.36	2.83	1.33	1.19	1.44	4.79	2.39	2.13
P_2O_5	0.04	0.03	0.08	0.09	0.06	0.11	0.03	0.07	0.15	0.25
LOI	0.54	0.57	0.39	0.44	0.75	1.52	1.03	0.69	0.25	0.50
SUM	98.79	99.58	99.70	99.11	99.07	99.90	100.12	99.34	99.31	99.12
SO_3	0.02	0.00	0.00	0.00	0.00	0.03	0.01	0.01	0.00	0.02
A/NK	1.83	1.60	1.99	1.71	2.00	2.57	2.19	1.41	1.83	1.81
A/CNK	1.05	1.06	1.05	1.05	1.05	0.94	0.94	1.04	0.98	0.90
$Mg^{\#}$	27	45	52	47	52	54	57	43	50	55
Na_2O/K_2O	3.79	2.93	3.11	1.20	3.31	4.22	3.49	0.68	1.40	1.90
Li	11.3	2.0	0.9	12.4	12.4	2.5	2.5	14.0	7.4	12.1
Be	1.02	0.87	0.73	1.06	0.86	0.99	1.10	1.00	1.01	1.36
Sc	1.5	1.7	1.9	3.4	1.9	2.2	2.8	3.0	10.9	9.3
Ti	171	1313	1762	1297	1059	1370	658	1125	2397	3053
V	3	23	36	30	17	33	18	23	77	81
Cr	12.8	8.1	12.2	34.2	5.6	13.1	26.2	5.7	83.4	90.9
Mn	43	88	194	264	156	259	316	120	430	477
Co	0.81	3.42	8.37	6.28	5.20	7.91	6.03	2.88	13.60	15.71
Ni	4.2	4.1	16.3	15.4	6.9	16.5	9.7	9.0	27.5	57.5
Cu	4.3	5.2	3.6	1.7	1.8	10.0	3.5	4.2	4.0	22.3
Zn	5	33	30	35	28	30	29	19	58	66
Ga	14.9	16.7	15.7	16.2	17.2	17.3	17.2	18.6	18.1	22.4
As	0.67	1.22	1.14	0.99	1.34	1.43	1.08	1.47	1.98	2.61
Se	0.09	0.08	0.08	0.25	0.16	0.23	0.28	0.21	0.58	0.72
Rb	11	11	37	53	26	17	15	111	44	34
Sr	383	1188	541	604	651	609	489	434	586	1062
Y	3.85	0.57	0.98	3.00	0.99	4.80	5.41	4.12	10.60	10.20
Zr	143	75	84	78	79	52	50	111	110	179
Nb	0.2	0.7	1.2	2.1	0.9	3.7	1.8	2.3	2.7	6.2
Mo	0.18	0.07	0.11	0.09	0.03	0.23	0.15	0.23	0.31	0.03
Cs	0.01	0.04	0.10	0.04	0.78	0.55	1.19	0.61	0.04	0.01
Ba	319	995	630	1225	483	186	340	1036	1026	1449
La	15.9	6.8	9.4	19.1	9.0	7.3	8.3	28.7	23.4	40.9
Ce	24	11	16	32	15	15	16	52	51	81
Pr	2.4	1.2	1.6	3.1	1.6	1.9	1.9	5.0	5.9	9.1
Nd	8	4	6	10	6	8	8	18	24	37
Sm	1.0	0.6	0.7	1.3	0.7	1.5	1.4	2.1	3.9	5.4
Eu	0.81	0.46	0.45	0.94	0.41	0.68	0.50	0.89	1.02	1.79
Gd	0.8	0.3	0.4	0.9	0.4	1.2	1.2	1.4	3.0	3.6
Tb	0.11	0.03	0.05	0.11	0.05	0.17	0.17	0.17	0.40	0.44
Dy	0.60	0.12	0.19	0.51	0.19	0.88	0.91	0.77	1.98	1.99
Ho	0.13	0.02	0.03	0.10	0.03	0.16	0.18	0.14	0.37	0.36
Er	0.37	0.06	0.10	0.30	0.10	0.43	0.49	0.38	1.02	0.97
Tm	0.06	0.01	0.01	0.04	0.01	0.06	0.07	0.05	0.14	0.13
Yb	0.37	0.05	0.09	0.31	0.09	0.39	0.47	0.32	0.89	0.84
Lu	0.06	0.01	0.01	0.05	0.01	0.06	0.07	0.05	0.12	0.12
Hf	3.81	1.81	1.96	1.86	1.98	1.43	1.39	2.92	2.83	4.14
Ta	0.03	0.35	0.06	0.12	0.02	0.24	0.12	0.09	0.13	0.21
Pb	6.2	6.9	3.8	11.0	4.1	5.2	5.8	11.7	9.8	9.4
Th	0.4	0.0	0.1	0.2	0.3	1.4	0.2	3.3	0.4	0.2
U	0.14	0.04	0.03	0.03	0.04	0.57	0.12	0.31	0.08	0.05
Sr/Y	99.56	2069.70	554.39	201.06	660.31	126.67	90.51	105.27	55.27	104.05
La/Sm	16.29	12.23	14.50	15.35	13.33	5.02	6.10	13.44	5.94	7.58
Yb_N	2.19	0.30	0.51	1.81	0.51	2.29	2.79	1.89	5.23	4.93
$(La/Yb)_N$	30.52	96.88	78.08	44.63	73.50	13.56	12.50	63.94	18.91	35.00
δEu	2.80	3.23	2.70	2.78	2.32	1.55	1.23	1.57	0.91	1.24
total HREE	2.50	0.64	0.89	2.29	0.92	3.38	3.53	3.30	7.91	8.49
total REE	55.00	24.68	34.24	68.73	33.55	38.30	39.07	109.24	117.21	183.30

TABLE 1

(continued)

Sample No.	17TX7	17TX10-2	17TX3-1	17TX4-2	17TX5-1	17TX6	17TX9	17TX10-1	17TX11-2	17TX11-5	17TX11-6	17TX11-8
						Dioritic gneisses					Gabbroic gneisses	
SiO_2	64.60	64.31	55.15	57.17	55.74	60.94	60.24	58.02	51.41	59.32	49.53	50.00
TiO_2	0.34	0.47	1.47	0.46	1.26	0.63	0.79	0.71	0.39	0.65	0.74	0.98
Al_2O_3	16.37	16.06	14.58	17.27	13.93	14.82	14.84	17.01	23.46	17.81	13.84	13.35
Fe_2O_3	4.44	3.94	10.67	10.21	10.90	6.72	8.97	7.17	4.41	6.05	14.22	15.09
MnO	0.07	0.06	0.15	0.24	0.24	0.09	0.12	0.11	0.06	0.09	0.22	0.23
MgO	2.43	2.00	4.20	3.45	5.08	3.85	3.53	3.77	2.82	3.18	7.32	6.42
CaO	4.96	5.29	6.33	5.46	8.05	5.57	6.65	6.37	8.54	5.53	10.48	10.32
Na_2O	3.84	4.08	3.12	3.18	2.87	3.22	3.23	4.28	4.04	4.38	2.40	2.98
K_2O	1.94	1.60	2.27	1.16	0.67	2.46	0.56	1.37	2.01	1.51	0.89	0.70
P_2O_5	0.12	0.19	0.83	0.13	0.10	0.23	0.18	0.24	0.02	0.26	0.10	0.10
LOI	0.62	1.56	0.20	0.63	1.07	0.69	0.13	0.28	2.31	0.51	0.41	0.18
SUM	99.73	99.55	98.97	99.35	99.91	99.22	99.24	99.33	99.47	99.29	100.15	100.33
SO_3	0.00	0.03	0.29	0.22	0.18	0.27	0.01	0.03	0.08	0.38	0.21	0.18
A/NK	1.94	1.90	1.92	2.67	2.56	1.86	2.51	2.00	2.66	2.01	2.81	2.36
A/CNK	0.94	0.89	0.76	1.05	0.69	0.82	0.82	0.85	0.96	0.94	0.58	0.55
$Mg^{\#}$	52	50	44	40	48	53	44	51	56	51	51	46
Na_2O/K_2O	1.98	2.55	1.37	2.75	4.30	1.31	5.72	3.11	2.01	2.90	2.69	4.26
Li	17.6	15.3	13.8	12.5	15.5	11.2	13.6	7.7	35.4	11.1	6.5	17.4
Be	0.91	1.17	1.85	1.11	0.80	1.00	0.68	1.24	1.27	1.29	0.56	0.67
Sc	15.3	8.4	20.7	19.2	38.4	18.2	22.6	16.4	7.7	16.0	46.7	49.6
Ti	1918	2801	8541	2680	7131	3654	4715	4096	2296	3828	4472	5877
V	82	74	179	91	331	135	160	149	64	136	292	329
Cr	135.1	89.3	107.7	125.9	113.1	259.0	63.5	109.1	50.4	153.4	109.9	39.0
Mn	487	434	1085	1693	1774	692	910	778	410	657	1672	1745
Co	12.65	13.60	31.05	19.85	40.40	26.19	24.32	25.04	15.34	26.34	59.85	56.46
Ni	36.8	38.4	53.4	42.8	57.9	83.7	52.4	47.0	41.3	77.4	81.8	49.5
Cu	5.9	11.7	70.3	29.8	36.2	64.6	33.2	48.0	23.5	101.2	54.1	53.2
Zn	54	52	114	71	112	79	67	87	53	95	105	114
Ga	18.6	19.6	24.9	19.3	19.3	19.1	16.1	21.8	19.9	23.1	15.8	17.6
As	1.45	2.24	4.32	2.06	1.64	2.31	1.66	2.25	1.90	2.53	1.36	2.09
Se	0.57	0.45	1.29	0.97	1.32	0.76	0.76	0.76	0.42	0.71	0.71	0.81
Rb	36	20	49	16	5	48	6	13	34	19	13	5
Sr	511	653	661	460	163	670	222	823	455	828	171	248
Y	11.23	8.45	27.66	25.05	32.79	16.37	24.74	15.00	10.94	13.09	19.15	24.67
Zr	68	172	234	72	147	135	132	104	95	155	47	47
Nb	3.1	4.3	12.8	4.9	7.0	6.2	5.9	6.2	5.0	5.3	3.2	2.9
Mo	0.08	0.07	0.85	0.54	0.49	0.32	0.43	0.18	0.29	0.14	0.24	0.30
Cs	0.59	1.11	0.37	0.08	0.02	0.85	0.59	0.97	2.64	0.45	0.73	0.24
Ba	850	768	1388	332	156	1121	161	690	313	664	108	214
La	16.5	22.2	56.8	14.8	9.7	23.9	10.4	24.1	10.0	23.0	8.8	11.8
Ce	35	47	119	39	24	58	24	58	22	55	20	28
Pr	3.9	5.1	13.7	5.2	3.5	7.2	3.4	7.1	2.9	6.7	2.6	3.7
Nd	16	21	57	24	16	31	16	30	13	31	11	16
Sm	3.0	3.1	9.0	5.0	4.0	5.3	3.5	5.2	2.6	5.1	2.4	3.2
Eu	1.09	1.27	2.47	1.21	1.26	1.56	1.01	1.41	0.72	1.56	0.85	1.10
Gd	2.7	2.4	7.2	4.8	4.7	4.3	3.8	4.0	2.3	3.9	2.8	3.6
Tb	0.39	0.32	0.96	0.75	0.84	0.57	0.64	0.54	0.34	0.50	0.48	0.63
Dy	2.11	1.54	4.90	4.24	5.44	3.05	3.97	2.73	1.89	2.47	3.08	4.04
Ho	0.41	0.29	0.95	0.85	1.18	0.60	0.85	0.53	0.38	0.46	0.66	0.87
Er	1.12	0.80	2.63	2.38	3.47	1.63	2.47	1.49	1.07	1.25	1.93	2.53
Tm	0.16	0.11	0.37	0.35	0.53	0.23	0.38	0.21	0.16	0.17	0.30	0.37
Yb	0.99	0.75	2.32	2.26	3.44	1.49	2.42	1.40	1.05	1.10	1.97	2.45
Lu	0.15	0.11	0.35	0.33	0.50	0.22	0.37	0.21	0.16	0.17	0.30	0.37
Hf	1.78	3.92	5.28	1.81	3.74	3.41	3.29	2.65	2.35	3.66	1.30	1.39
Ta	0.10	0.19	0.62	0.18	0.36	0.27	0.40	0.27	0.30	0.14	0.18	0.25
Pb	5.7	6.4	10.9	5.1	2.2	6.3	1.6	5.7	4.6	7.1	1.9	3.1
Th	0.1	0.2	1.4	0.2	0.3	0.1	0.2	0.1	1.4	0.1	0.9	0.1
U	0.07	0.06	0.33	0.07	0.10	0.11	0.08	0.05	0.41	0.06	0.08	0.01
Sr/Y	45.55	77.28	23.89	18.37	4.96	40.94	8.96	54.88	41.63	63.22	8.95	10.04
La/Sm	5.44	7.07	6.33	2.93	2.42	4.48	2.94	4.64	3.87	4.52	3.61	3.73
Yb_N	5.83	4.41	13.63	13.27	20.25	8.76	14.21	8.21	6.15	6.45	11.57	14.43
$(La/Yb)_N$	11.91	21.19	17.58	4.69	2.01	11.51	3.07	12.38	6.82	15.05	3.22	3.44
δEu	1.18	1.41	0.94	0.76	0.90	1.00	0.84	0.95	0.91	1.08	0.99	0.99
total HREE	7.98	6.33	19.69	15.93	20.08	12.09	14.90	11.10	7.34	9.97	11.53	14.90
total REE	83.48	105.99	277.32	105.35	78.22	139.27	73.38	137.84	58.41	131.68	57.38	78.68

Notes: Mg# = 100 Mg/(Mg + Fe_{total}) in atomic ration; $\delta Eu = Eu_N/\text{sqrt}(Sm_N \times Gd_N)$; subscript N-chondrite normalized value.

63.94 (table 1). As shown in the primitive mantle-normalized trace element spidergram (fig. 5B), the low-Yb gneisses have negative anomalies of Nb, Ta, Ti, and P. By contrast, Zr and Hf display positive or no anomalies. All the normalized Yb contents are lower than 1, elevating $(La/Yb)_N$ values (average of 51.70). The normalized Y

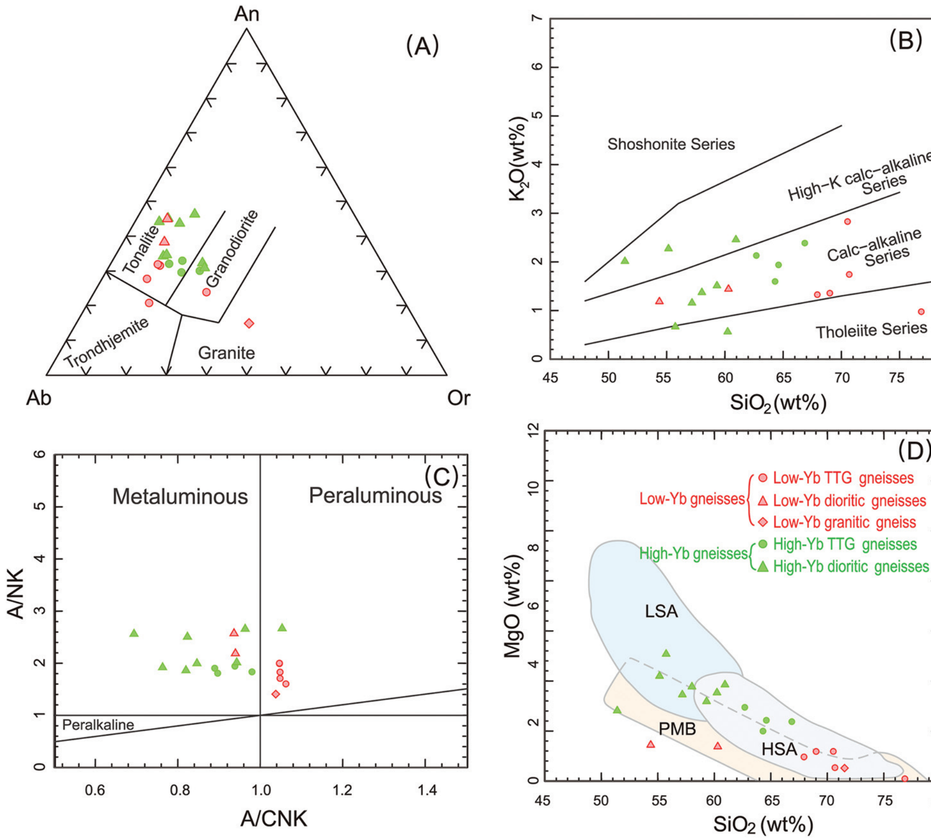

Fig. 4. Major element compositions and geochemical classifications of the Tianzhen gneisses from the Huai'an Complex, which are subdivided into the high-Yb gneisses and the low-Yb gneisses. (A) An–Ab–Or classification diagram (after Barker, 1979); (B) K_2O versus SiO_2 classification diagram (after Peccerillo and Taylor, 1976); (C) A/NK (molecular $Al_2O_3/(Na_2O + K_2O)$) versus A/CNK (molecular $Al_2O_3/(CaO + Na_2O + K_2O)$) classification diagram (after Maniar and Piccoli, 1989); (D) MgO versus SiO_2 diagram (after Martin and others, 2005). Abbreviations: PMB – experiment-derived partial melts from metabasaltic rocks; LSA – low silica adakite; HSA – high silica adakite.

contents are also lower than 1.5, resulting in high Sr/Y ratios (average of 488). The low-Yb gneissic samples are rich in large ion lithophile elements (LILE, including Rb, K, Sr, and Ba), but show low contents of Cr (5.6–34.2 ppm), Co (0.81–8.37 ppm), and V (3–36 ppm) (table 1).

The high-Yb gneisses.—In the chondrite-normalized REE patterns, the high-Yb gneisses show fractionated REE patterns with less depleted HREE contents than low-Yb gneisses. Most high-Yb gneisses have no Eu anomalies except for two TTG gneisses that show weakly positive Eu anomalies (fig. 5A). Among the high-Yb gneissic samples, four TTG gneisses have HREE and REE contents of 6.33 to 8.49 and 83.48 to 183.30 ppm with δEu (Eu/Eu*) ratios of 0.91 to 1.41 and $(La/Yb)_N$ values of 11.91 to 35.00, while another eight dioritic gneisses have higher HREE and REE contents of 7.34 to 20.08 and 58.41 to 277.32 ppm, respectively, with lower δEu (Eu/Eu*) ratios of 0.76 to 1.08 and $(La/Yb)_N$ values of 2.01–17.58. In addition, the two gabbroic gneisses have HREE and REE contents of 11.53 to 14.90 and 57.38 to 78.68 ppm, respectively, with the δEu (Eu/Eu*) ratios of 0.99 and $(La/Yb)_N$ values of 3.22 to 3.44, respectively (table 1).

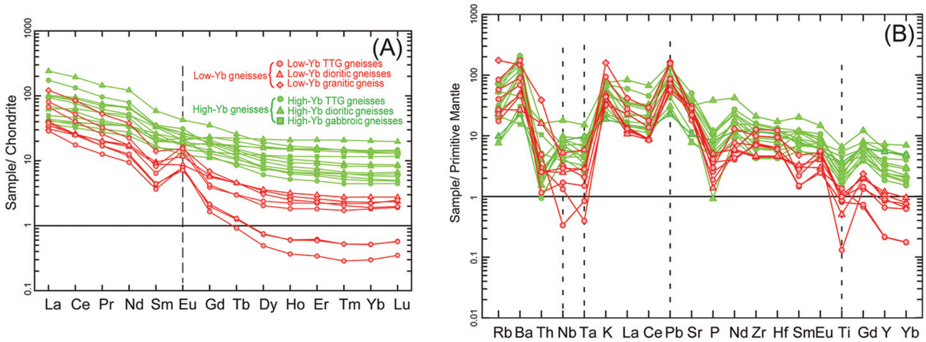

Fig. 5. Chondrite-normalized REE diagram (A) and Primitive mantle-normalized trace element spidergram (B) for the Tianzhen gneisses from the Huai'an Complex, which are subdivided into the high-Yb gneisses and the low-Yb gneisses. Chondrite and primitive mantle normalizing values are from Sun and McDonough (1989).

In the primitive mantle-normalized trace element spidergram (fig. 5B), the high-Yb gneisses display relatively lower negative anomalies of Nb, Ta, Ti, and P than the low-Yb gneisses. Zr and Hf anomalies are not conspicuous. All the normalized Yb contents are higher than 1, causing lower $(La/Yb)_N$ values (average of 11.91). The normalized Y contents are also higher than 1.5, resulting in lower Sr/Y ratios (average of 39.86). The high-Yb gneissic samples show slightly higher Rb and K than the low-Yb samples but reveal not much difference in Sr and Ba compositions. High contents of Cr (39.0–259.0 ppm), Co (12.65–59.85 ppm), and V (64–331 ppm) were obtained (table 1).

DISCUSSION AND IMPLICATIONS

Petrogenesis of the Huai'an Gneisses

Petrogenesis of the Huai'an low-Yb gneisses.—The low-Yb gneisses vary between intermediate and felsic, represented by a majority of the TTG rocks and some of the dioritic gneisses and the granitic gneiss. The low-Yb gneisses mostly plot in the high-Si adakite (HSA) field, with low MgO forming a negative correlation with SiO_2 (fig. 4D). In general, the low-Yb gneiss samples show Mg# analogous to typical subducted oceanic crust-derived adakite, although with a wider range of SiO_2 (fig. 6A). Most samples plot above the field of experiment-derived melts from metamorphosed basalts or eclogites, indicating the involvement of mantle materials (Stern and Kilian, 1996; Rapp and others, 1999; Smithies, 2000). One view is that adakite is derived from subducted slab melts whose composition has been modified by interaction with mantle peridotite, accounting for its relation with subduction zones (Maury and others, 1996; Prouteau and others, 2001; Martin and others, 2005). Accordingly, the low-Yb gneisses with adakite-affinity could be related to interaction of slab-derived melt with the overlying mantle wedge during ascent. Alternatively, adakite may result through melting of basalts underplated beneath continental crust (Atherton and Petford, 1993; Kay and others, 1993; Petford and Atherton, 1996). However, the lack of interaction between felsic melts and mantle peridotite would lead to low Mg# values and low Cr and Ni concentrations, which is inconsistent with results of the low-Yb gneisses in this study (average Mg#, Cr, and Ni of 47.09, 14.75 ppm, and 10.24 ppm, respectively). In addition, basalt melting experiments performed by Prouteau and others (2001) indicated that trondhjemitic melts are only generated when free water is available.

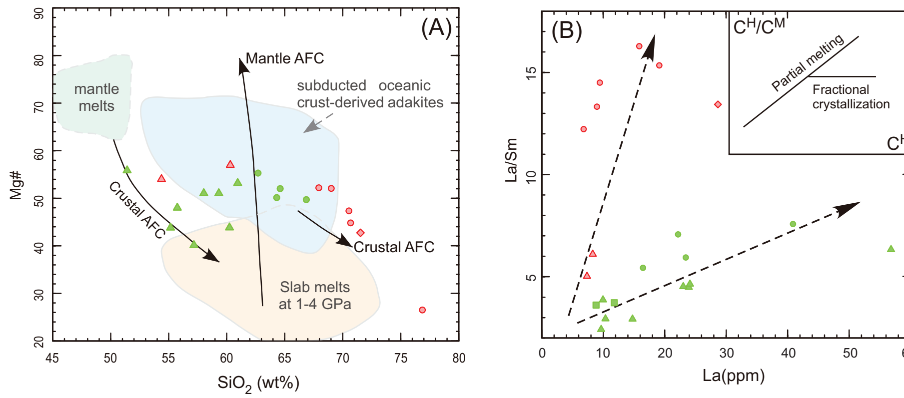

Fig. 6. Petrogenetic diagrams for the Tianzhen gneisses, indicating their derivation from partial melting of subducted oceanic slab and interaction with the overlying mantle wedge. (A) Mg# (molecular 100 Mg/(Mg + Fe_{total})) versus SiO_2 diagram (reference fields for slab experimental melts at 1 to 4 GPa after Rapp and others (1999), and for subducted oceanic crust-derived adakites after Liu and others (2012d), and for mantle melts and curves after Stern and Kilian (1996)). Abbreviations: AFC –assimilation and fractional crystallization; (B) La/Sm versus La diagram (Treuil M, 1975; Allegre and Minster, 1978; Hofmann and Feigenson, 1983; Schiano and others, 2010); the inset is a schematic C^H/C^M versus C^H diagram, where H and M are highly incompatible and moderately incompatible elements, respectively. Symbols are the same as in figure 5.

Dehydration melting in the garnet field of underplated basalt would give rise to magma with less-sodic compositions, which is not the case for the studied low-Yb gneisses, some of which are trondhjemite.

Experimental studies have shown that garnet plays an important role in controlling REE distribution in melts, because HREEs are strongly compatible in garnet relative to other REEs (Rushmer, 1991; Rollinson, 2014). In this case, the highly depleted HREEs (fig. 5A) in the low-Yb gneisses indicate that the low-Yb magma was in equilibrium with garnet. Relative to HREEs, MREEs are more compatible in amphibole (Rollinson, 2014). Associated with the relatively flat fractionated REE patterns, amphibole and garnet were supposed to be residual during partial melting. On the other hand, positive Eu anomalies are characteristic of the low-Yb gneisses (fig. 5A) together with high concentrations of Sr (383 to 1188 ppm) (table 1). Plagioclase should not have been a residual phase because it is the main phase that controls Sr concentration and Eu anomaly (Martin, 1987; Springer and Seck, 1997). A high-pressure origin becomes implicit, as plagioclase undergoes breakdown during partial melting at high pressures (Goldsmith, 1980). This trace element signature also makes "Archean TTG" different from modern continental crust, which has higher HREE contents (for example, $Yb_{average}$=3.26 ppm) and negative Eu, Nb, Ta, Sr, and Ti anomalies (Moyen and Martin, 2012). In the primitive-mantle-normalized trace element spidergram (fig. 5B), the negative Nb, Ta, and Ti anomalies and moderately positive Pb anomalies are typical characteristics of subduction-related magmas. Although Ti, Nb, and Ta could be held by amphibole (Tiepolo and others, 2000; Foley and others, 2002; Foley, 2008), the marked negative anomalies of these components may be chiefly ascribed to residual Ti-bearing mineral phases, like rutile, titanite, or ilmenite (Foley and others, 2000; Schmidt and others, 2004; Klemme and others, 2005; Xiong and others, 2005, 2009; Xiong, 2006).

Figure 6B shows that the low-Yb gneisses were not generated by magma mixing or fractional crystallization but by partial melting (Treuil M, 1975; Allegre and Minster, 1978; Hofmann and Feigenson, 1983; Schiano and others, 2010). The $(La/Yb)_N$ versus $(Yb)_N$ diagram (fig. 7A) shows affinity between the low-Yb gneisses and Archean

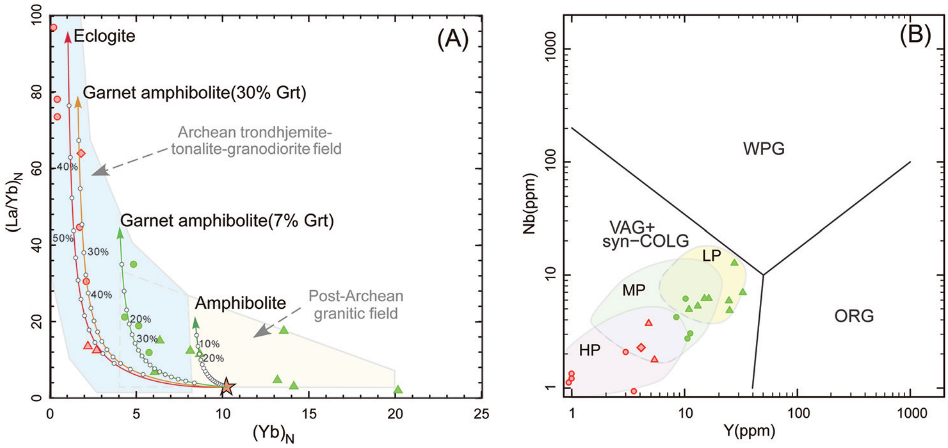

Fig. 7. Petrogenetic diagrams for the Tianzhen gneisses, indicating their derivation from partial melting of subducted oceanic slab with various mineral compositions under a range of pressures. (A) $(La/Yb)_N$ versus $(Yb)_N$ diagram. Partial melting curves are calculated for batch melting of the average Archaean tholeiite (La = 6.873 ppm, Yb = 1.751ppm) (Martin, 1987). Melt fractions of 5%, 10%, 20%, 30% and 50% are represented by white circles on each of the model curves. The Archean trondhjemite-tonalite-granodiorite field and post-Archean granitic field are modified from Petford and Atherton (1996), subscript N represents chondrite normalized value and chondrite normalizing values are from Sun and McDonough (1989). The details of trace element modeling see table A1; (B) Nb versus Y diagram (Pearce and others, 1984), discriminating different groups of TTG series (reference fields for high/medium/low-pressure TTG rocks after Moyen (2011)). Abbreviations: VAG – volcanic-arc granite, Syn-COLG – syn-collision granite, WPG – within-plate granite, ORG – ocean-ridge granite, HP – high pressure TTG series, MP – middle pressure TTG series, LP – low pressure TTG series. Symbols are the same as Fig. 4.

adakite. Wide variations of $(La/Yb)_N$ ratios with notably low $(Yb)_N$ are recorded, which suggests that the low-Yb melts should have formed from the partial melting of eclogite or 30% garnet-bearing amphibolite (Petford and Atherton, 1996; Moyen and Stevens, 2006; Moyen and Martin, 2012).

Gneisses from the low-Yb group plot in the field of "Volcanic Arc Granite" in figure 7B, indicating that they were generated in a volcanic arc setting. In addition, the low-Yb samples not only show significantly low Y and Nb contents but also fall into the area of medium-pressure (MP) (*ca.* 15 kbar) to high-pressure (HP) (>20 kbar) TTG series based on the TTG division of Moyen (2011). It should be also noted that high pressures of about 20 kbar are unlikely to be achieved within the crust, especially in a weaker Archean crust.

Petrogenesis of the Huai'an high-Yb gneisses.—The high-Yb gneisses are dominated by intermediate to felsic rocks, together with two gabbroic gneisses. Exhibiting higher MgO compositions than the low-Yb gneisses, the high-Yb gneisses plot in the field of both HSA and low-Si adakite (LSA) (fig. 4D). In the Mg#-SiO_2 plot, the high-Yb gneisses resembles the low-Yb group despite more concentrated SiO_2 compositions (fig. 6A). Experimental studies demonstrate that partial melting of hydrous basaltic rocks leads to magmas characterized by low Mg# (<45) regardless of pressure conditions of melting (Rapp and Watson, 1995; Rapp and others, 1999). The high-Yb gneisses have relatively higher Mg# values than melts from metabasaltic rocks at a given silica content and show affinity with subducted oceanic crust-derived adakite in the Mg# versus SiO_2 diagram (fig. 6A), similar to the low-Yb gneisses. The high-Yb gneisses could also result from interaction of slab-derived melt with mantle peridotite. Additionally, the higher Mg# values and much higher Cr and Ni concentrations of the high-Yb gneisses can be ascribed to contamination by mantle during ascent of slab melts (Smithies and Champion, 2000; Martin and Moyen, 2002; Martin and others, 2005; Rapp and others, 2010).

The high-Yb gneisses display fractionated REE patterns but higher HREE compositions (such as Yb and Y) than the low-Yb group (fig. 5A), indicating that residual garnet and amphibole should be left during the partial melting of oceanic crust. With higher HREE contents (for example, $Yb_{average}$ = 1.67 ppm), the high-Yb gneisses are distinct from the modern continental crust (for example, $Yb_{average}$ = 3.26 ppm) (Moyen and Martin, 2012). There are slightly positive or no Eu anomalies (fig. 5A) and high concentrations of Sr (163 to 1061 ppm), supporting a similar lack of residual plagioclase to that of the low-Yb gneisses. Although the Nb, Ta, and Ti compositions of the high-Yb gneisses are higher than those of the low-Yb group, the negative Nb, Ta, and Ti anomalies and positive Pb anomalies (fig. 5B) are indicative of subduction-related magma. Ti-bearing minerals might also be residual to account for the Nb, Ta, and Ti depletions. In addition, the two gabbroic gneisses exhibit high Ba/La (18.13 and 12.23) but low Th/Yb ratios (0.03 and 0.45), reflecting a dominant contribution from hydrous (slab-derived) fluids (Woodhead and others, 2001).

The positive correlation between La/Sm ratios and La (similarly Ta/Sm ratios and Ta) (fig. 6B) reveal partial melting as the major petrogenetic mechanism for the high-Yb gneisses, whereas the lower slope leads to a trajectory distinct from the low-Yb gneisses, which indicate that the two groups of samples were formed by partial melting in different conditions (Defant and Drummond, 1990). As indicated by the $(La/Yb)_N$ versus $(Yb)_N$ plot, partial melting trends from a basalt source that is garnet-free or 7% garnet-bearing amphibolite could account for the geochemical characteristics of the high-Yb gneisses, leading to much lower $(La/Yb)_N$ ratios than those of the low-Yb gneisses (fig. 7A). A volcanic arc tectonic environment for the high-Yb gneisses is also indicated by the Nb versus Y diagram (fig. 7B). Difference between the high-Yb and low-Yb gneisses appears in the Nb versus Y plot, because the high-Yb gneisses are akin to the Archean TTG series generated under low pressure (LP) (10–12 kbar) to medium pressure (MP) (*ca.* 15 kbar) (Moyen, 2011).

Neoarchean-Paleoproterozoic Tectonomagmatic Evolution of the TNCO

Evidence for magmatic arc development in the Huai'an Complex.—Irrespective of various genetic models, TTGs were generally derived from the partial melting of hydrous basaltic rocks under sufficiently high pressures (Defant and Drummond, 1990; Atherton and Petford, 1993; Martin and others, 2005; Moyen and Martin, 2012; Zhang and others, 2012a). Alternate models attribute their origins to partial melting from hot subducted slabs (Martin, 1986, 1999; Martin and Moyen, 2002; Foley and others, 2002), underplating or intraplating of hydrous basaltic lower crust (Smithies, 2000; Whalen and others, 2002; Chung and others, 2003; Condie, 2005), or fractionated hydrous mantle wedge-derived melts (Kamber and others, 2002; Kleinhanns and others, 2003).

TTGs appear to be a composite rock suite that formed at a range of pressures from <10 to >25 kbar (Moyen, 2011). The Huai'an gneisses in this study belong to TTG series, which is divisible into the low-Yb and high-Yb gneisses. The diverse geochemical features between the two groups can be interpreted to result from different petrogenesis, including diverse source compositions and pressure conditions.

Some of the samples in this study have undergone the U-Pb dating and isotopic analyses in a previous study (Zhao and others, 2020), which show that the plutonic protoliths of the Huai'an gneisses were emplaced at 2.51 to 2.40 Ga and experienced a metamorphic event at 1.86 to 1.80 Ga. The positive $\varepsilon_{Hf}(t)$ values from +1.9 to +7.0 also suggest derivation of their precursor magmas from juvenile crust (Zhao and others, 2020). In accordance with geochemical features mentioned in Section 5.1, the Huai'an low-Yb gneisses are considered to form by the partial melting of subducted oceanic crust consisting of eclogite or 30% garnet-bearing amphibolite between 15 and 20 kbar or even higher pressure, with garnet, amphibole, and rutile as residues. Conversely, the high-Yb TTG magma was derived from the partial melting of a subducted oceanic slab that was garnet-free or composed of 7% garnet amphibole between 10 and 15 kbar, leaving residual garnet and amphibole. Both magmas were then interacted with the overlying mantle wedge during ascent.

A similar tectonic process is supported by the geochemical behavior of gneisses from the Huai'an Complex in the study of Liu and others (2012d), which divided TTG gneisses into TTG and dioritic series and considered them to resemble adakite and sanukitoid, respectively. In my view, considering the lower MgO (<6 wt%) and Rb compositions and slightly positive Sr anomalies of the dioritic gneisses, both series are more analogous to Archean adakite (Martin and others, 2005). In addition, the negative Nb, Ta, and Ti anomalies and low Y contents of his samples are important evidence to support a subduction origin.

In addition to geochemical features, there are other features consistent with crust-mantle evolution and interaction processes.

Most Huai'an gneisses display a gneissic structure defined by oriented biotite and a lineation defined by oriented hornblende. In the Huai'an Complex, late Archean to Paleoproterozoic basement is generally characterized by linear belts (Dirks and others, 1997; Zhao and others, 2008a). A magmatic arc regime with later continent-continent collision can also explain the recognition of high-pressure pelitic granulites and clockwise P–T paths for granulites from the Huai'an Complex (Guo and others, 1993; Wu and others, 2016).

According to geochronological studies (Su and others, 2014; Zhao and others, 2020), no inherited zircons are preserved in the Huai'an gneisses, indicating no contamination by ancient continental crust. This is in sharp contrast to the contemporaneous ~2.5 Ga gneisses in most complexes of the TNCO (for example, the Fuping Complex, Hengshan Complex, Taihua Complex; Zhao and others, 2002b; Kröner and others, 2005b; Liu and others, 2009a; Han and others, 2012) and >2.7 Ga rocks in the interior of the EB (for example, the Eastern Hebei terrane, Eastern Shandong terrane, Jiaobei terrane; Liu and others, 2013b; Wu and others, 2014; Duan and others, 2017; Guo and others, 2017). Furthermore, the positive zircon $\varepsilon_{Hf}(t)$ values (+1.9 to +7.0) together with the whole-rock $\varepsilon_{Nd}(t)$ values (+0.8 to +4.3) (Liu and others, 2009b; Zhao and others, 2020) suggest that the gneisses from the Huai'an Complex were derived from partial melting of juvenile crust, whose magmas were extracted from depleted mantle, and there was no involvement of old continental crust during this process (Wu and others, 2005; Geng and others, 2012). Therefore, the protoliths of the Huai'an gneisses are products of arcs, and an intra-oceanic arc setting is considered likely for the Huai'an Complex.

Based on the lithological, geochemical and petrogenetic investigation of the gneisses of the Huai'an Complex in the TNCO, we propose that the Neoarchean TTG series gneisses were generated in a magmatic arc tectonic setting and oceanic subduction. Although an intra-oceanic arc setting is preferred to interpret the isotopic characteristics, more available data are required to support a Japan-type island arc and preclude an Andean-type continental margin magmatic arc setting during the Neoarchean to Paleoproterozoic (2.5 Ga–1.8 Ga).

Geodynamic Implication for a magmatic arc system in the TNCO.—The above magmatic arc regime is consistent with the oceanic subduction model that has been applied to other complexes throughout the TNCO, as proposed by previous researchers (Kröner and others, 2005a, 2005b; Zhou and others, 2009; Huang and others, 2010).

Similar geochemical features were determined in other areas, like Hengshan, Wutai, and Dengfeng, supporting an arc derivation (Sun and others, 1992; Liu and others, 2002, 2004, 2012c; Zhao and others, 2007). The Neoarchean to Paleoproterozoic basement in the TNCO is generally characterized by linear structural belts that were deformed at ~1.8 Ga (Zhang and others, 2009, 2012b; Trap and others, 2012). In a few domains, such as the Fuping and Dengfeng, where voluminous reworked Archean gneisses and mafic granulites are exposed, small gneiss domes occur within the linear belts, and their orientation is subparallel to the regional foliation (Zhao and others, 2001b). These structures are consistent with the expected horizontal tectonic movement during the subduction process in the TNCO. Another piece of lithological evidence is the 1.9 to 1.8 Ga high-pressure rocks distributed across the TNCO, including HP pelitic granulites in the northern sector, which are generally considered to define subduction/collision belts (Zhai and others, 1992, 1995; Guo and others, 1993, 2001, 2002; Zhao and others, 2001a, 2006; Zhang and others, 2006; Xiao and others, 2011). In addition, contemporaneous juvenile crustal growth (2.8–2.6 Ga) and important magmatic events (~2.5 Ga) are recorded in other complexes along the TNCO (Zhou and others, 2009; Diwu and others, 2011; Zhai and Santosh, 2011; Geng and others, 2012).

A possible intra-oceanic arc tectonic model has been applied to the metamorphic complexes, like the Huai'an and Xuanhua complex (Liu and others, 2006; Wang and others, 2015), while other metamorphic complexes such as the Lüliang, Hengshan, Fuping, and Dengfeng complexes in the TNCO formed in an active continental margin arc between the ocean and the Eastern Block, or the ocean and the Western Block (Faure and others, 2007; Zhao and others, 2007, 2008b; Santosh, 2010a; Diwu and others, 2011; Kusky and others, 2016). It is concluded that these complexes in the TNCO represent a single, long-lived Neoarchean to Paleoproterozoic magmatic arc (Zhao and others, 2007).

Based on the lithological, geochemical, and geochronological studies, the tectonic scenario for the TNCO during Neoarchean to Paleoproterozoic time is suggested as follows:

1. Initially, the Eastern and Western Blocks were separated by an ancient ocean and then the oceanic lithosphere began to subduct (eastward or westward) in the Neoarchean to Paleoproterozoic. In the subduction process, the partial melting of subducted oceanic slabs generated a large amount of magma, which interacted with the overlying mantle wedge during ascent. The magmas crystallized to form TTG, dioritic, gabbroic, and granitic rocks, leading to the formation of juvenile continental crust.
2. The long-lived magmatic arc was terminated at ~1.8 Ga, by final closure of the ocean triggering continent-continent collision between the Eastern Block and the Western Block, forming the TNCO. In this scenario, the TTG series underwent upper amphibolite- to granulite-facies metamorphism.

CONCLUSIONS

The Tianzhen gneisses of the TTG series from the Huai'an Complex are divisible into low-Yb and high-Yb gneisses, both of which were derived from the partial melting of subducted oceanic slabs and the magmas then interacted with the overlying mantle wedge during magma ascended.

The diverse geochemical features between the low-Yb and high-Yb groups can be interpreted to result from different source materials and pressure conditions. The low-Yb gneisses are considered to be derived from eclogite or 30% garnet-bearing amphibolite, whereas the high-Yb gneisses were derived from garnet-free or 7% garnet-bearing amphibolite, both of which left unmelted garnet and amphibole as residues.

The Nb and Y compositions indicate that the former was produced between 15 to 20 kbar or even higher pressure, while the latter was generated at lower pressure of about 10 to 15 kbar.

The Huai'an Complex is considered to have been generated in an oceanic subduction setting leading to formation of juvenile continental crust during Neoarchean to Paleoproterozoic time. Integrated with recent studies on other complexes of the TNCO, a Neoarchean to Paleoproterozoic magmatic arc system is established along the TNCO.

ACKNOWLEDGMENTS

This paper is in memory of Prof. Alfred Kröner who had long collaborations with our group on the Precambrian geology of the North China Craton. Suggestions by Dr. Qian Liu are gratefully acknowledged that led to improvement of the manuscript. We appreciate Linqing Li at the Hebei Geology and Resource Bureau in Langfang for assistance in sample preparation. We also give thanks to Jianfeng Gao, Liang Li and Rangtian Wu at Nanjing FocuMS Technology Co. Ltd. for their help during the whole-rock major and trace element analyses. Reviews by two anonymous reviewers and Dr. Simon Wilde are thankfully acknowledged for their constructive comments and suggestions that improved the manuscript a lot. This study was financially supported by the sub-project of an NSFC Major Project, entitled "Continental Crust Growth-Stabilization and Initiation of the Early Plate Tectonics" (Project Code: 41890831). This paper is a contribution of the Chemical Geodynamic Joint Laboratory between HKU and Guangzhou Institute of Geochemistry, CAS.

APPENDIX

Table A1

Partition coefficients and trace element modeling for the partial melting of the TTG source

Source		**Partition coefficients**			**proportions of mineral assemblages**			
					eclogite	**garnet amphibolite (30%)**	**garnet amphibolite (7%)**	**amphibolite**
La	6.873	**Cpx**	0.1	0.6	35	15	10	5
Yb	1.751	**Grt**	0.04	21	60	30	7	0
Yb_N	10.3	**Amp**	0.2	1.7	0	40	60	70
$(La/Yb)_N$	2.815534	**Pl**	0.13	0.024	0	15	18	15
		Rt	0.0057	0.0126	5	0	0	0
		Qtz	0.015	0.017	0	0	5	10
degree of partial melting	**eclogite**		**garnet amphibolite (30%)**		**garnet amphibolite (7%)**		**amphibolite**	
	$(Yb)_N$	**$(La/Yb)_N$**	**$(Yb)_N$**	**$(La/Yb)_N$**	**$(Yb)_N$**	**$(La/Yb)_N$**	**$(Yb)_N$**	**$(La/Yb)_N$**
0.01	0.81	520.24	1.47	145.70	4.06	43.16	8.42	19.72
0.05	0.84	323.61	1.52	111.83	4.16	34.99	8.48	16.44
0.10	0.89	213.51	1.59	85.03	4.29	27.98	8.56	13.56
0.15	0.93	155.10	1.67	67.31	4.44	23.05	8.64	11.51
0.20	0.99	118.90	1.76	54.73	4.59	19.39	8.73	9.98
0.25	1.04	94.26	1.85	45.32	4.75	16.58	8.81	8.78
0.30	1.11	76.41	1.96	38.03	4.93	14.34	8.90	7.83
0.35	1.19	62.88	2.08	32.22	5.12	12.52	8.98	7.05
0.40	1.27	52.27	2.22	27.47	5.33	11.01	9.07	6.40
0.45	1.37	43.73	2.37	23.51	5.55	9.74	9.16	5.84
0.50	1.49	36.71	2.55	20.17	5.79	8.65	9.26	5.37
0.55	1.63	30.83	2.76	17.31	6.06	7.71	9.35	4.96
0.60	1.80	25.84	3.00	14.84	6.35	6.89	9.45	4.60
0.65	2.01	21.55	3.30	12.67	6.67	6.17	9.55	4.29
0.70	2.27	17.82	3.65	10.77	7.02	5.53	9.65	4.01
0.75	2.61	14.55	4.09	9.07	7.42	4.95	9.75	3.76
0.80	3.06	11.66	4.65	7.56	7.86	4.44	9.86	3.53
0.85	3.72	9.09	5.39	6.19	8.35	3.97	9.96	3.33

Noted: the partition coefficients (D) for Cpx, Grt, Amp and Pl are from Martin, 1987. D for Rt from Xiong and others, 2005. D for Qtz from Bedard, 2006.

References

Allegre, C., and Minster, J., 1978, Quantitative models of trace element behavior in magmatic processes: Earth and Planetary Science Letters, v. 38, n. 1, p. 1–25, https://doi.org/10.1016/0012-821X(78)90123-1

Arndt, N. T., 1983, Role of a thin, komatiite-rich oceanic crust in the Archean plate-tectonic process: Geology, v. 11, n. 7, p. 372–375, https://doi.org/10.1130/0091-7613(1983)11<372:ROATKO>2.0.CO;2

Atherton, M. P., and Petford, N., 1993, Generation of sodium-rich magmas from newly underplated basaltic crust: Nature, v. 362, p. 144–146, https://doi.org/10.1038/362144a0

Barbarin, B., 1999, A review of the relationships between granitoid types, their origins and their geodynamic environments: Lithos, v. 46, n. 3, p. 605–626, https://doi.org/10.1016/S0024-4937(98)00085-1

Barker, F., 1979, Trondhjemite: definition, environment and hypotheses of origin, Developments in petrology, Elsevier, p. 1–12, https://doi.org/10.1016/B978-0-444-41765-7.50006-X

Bédard, J. H., 2006, Trace element partitioning in plagioclase feldspar: Geochimica et Cosmochimica Acta, v. 70, n. 14, p. 3717–3742, https://doi.org/10.1016/j.gca.2006.05.003

Belousova, E. A., Kostitsyn, Y. A., Griffin, W. L., Begg, G. C., O'Reilly, S. Y., and Pearson, N. J., 2010, The growth of the continental crust: Constraints from zircon Hf-isotope data: Lithos, v. 119, n. 3–4, p. 457–466, https://doi.org/10.1016/j.lithos.2010.07.024

Caro, G., Bourdon, B., Wood, B. J., and Corgne, A., 2005, Trace-element fractionation in Hadean mantle generated by melt segregation from a magma ocean: Nature, v. 436, p. 246–249, https://doi.org/10.1038/nature03827

Chung, S. L., Liu, D. Y., Ji, J. Q., Chu, M. F., Lee, H.Y., Wen, D. J., Lo, C. H., Lee, T. Y., Qian, Q., and Zhang, Q., 2003, Adakites from continental collision zones: Melting of thickened lower crust beneath southern Tibet: Geology, v. 31, n. 11, p. 1021–1024, https://doi.org/10.1130/G19796.1

Condie, K. C., 1998, Episodic continental growth and supercontinents: a mantle avalanche connection? Earth and Planetary Science Letters, v. 163, n. 1–4, p. 97–108, https://doi.org/10.1016/S0012-821X(98)00178-2

Condie, K.C., 2005, TTGs and adakites: are they both slab melts? Lithos, v. 80, n. 1–4, p. 33–44, https://doi.org/10.1016/j.lithos.2003.11.001
Condie, K. C., and Kröner, A., 2008, When did plate tectonics begin? Evidence from the geologic record, *in* Condie, K. C., and Pease, V., editors, When Did Plate Tectonics Begin on Planet Earth?: Geological Society of America, Special Paper, v. 440, p. 281–294, https://doi.org/10.1130/2008.2440(14)
Condie, K. C., and Kröner, A., 2013, The building blocks of continental crust: Evidence for a major change in the tectonic setting of continental growth at the end of the Archean: Gondwana Research, v. 23, n. 2, p. 394–402, https://doi.org/10.1016/j.gr.2011.09.011
Cui, W. Y., Wang, C. Q., and Wang, S. G., 1991, Geochemistry and metamorphic P-T-t path of the Jianping Complex in the western Liaoning Province: Acta Petrologica Sinica, v. 7, p. 13–26.
Defant, M. J., and Drummond, M. S., 1990, Derivation of some modern arc magmas by melting of young subducted lithosphere: Nature, v. 347, p. 662–665, https://doi.org/10.1038/347662a0
Dhuime, B., Hawkesworth, C. J., Cawood, P. A., and Storey, C. D., 2012, A Change in the Geodynamics of Continental Growth 3 Billion Years Ago: Science, v. 335, n. 6074, p. 1334–1336, https://doi.org/10.1126/science.1216066
Dirks, P. H. G. M., Zhang, J. S., and Passchier, C. W., 1997, Exhumation of high-pressure granulites and the role of lower crustal advection in the North China Craton near Datong: Journal of Structural Geology, v. 19, n. 10, p. 1343–1358, https://doi.org/10.1016/S0191-8141(97)00044-8
Diwu, C. R., Sun, Y., Guo, A. L., Wang, H. L., and Liu, X. M., 2011, Crustal growth in the North China Craton at ~2.5Ga: Evidence from in situ zircon U–Pb ages, Hf isotopes and whole-rock geochemistry of the Dengfeng complex: Gondwana Research, v. 20, n. 1, p. 149–170, https://doi.org/10.1016/j.gr.2011.01.011
Duan, Z. Z., Wei, C.J., and Rehman, H. U., 2017, Metamorphic evolution and zircon ages of pelitic granulites in eastern Hebei, North China Craton: Insights into the regional Archean P–T–t history: Precambrian Research, v. 292, p. 240–257, https://doi.org/10.1016/j.precamres.2017.02.008
Faure, M., Trap, P., Lin, W., Monié, P., and Bruguier, O., 2007, Polyorogenic evolution of the Paleoproterozoic Trans-North China Belt —New insights from the Lüliangshan-Hengshan-Wutaishan and Fuping massifs: Episodes Journal of International Geoscience, v. 30, n. 2, p. 96–107, https://doi.org/10.18814/epiiugs/2007/v30i2/004
Foley, S. F., 2008, Rejuvenation and erosion of the cratonic lithosphere: Nature Geoscience, v. 1, p. 503–510, https://doi.org/10.1038/ngeo261
Foley, S. F., Barth, M. G., and Jenner, G. A., 2000, Rutile/melt partition coefficients for trace elements and an assessment of the influence of rutile on the trace element characteristics of subduction zone magmas: Geochimica et Cosmochimica Acta, v. 64, n. 5, 933–938, https://doi.org/10.1016/S0016-7037(99)00355-5
Foley, S., Tiepolo, M., and Vannucci, R., 2002, Growth of early continental crust controlled by melting of amphibolite in subduction zones: Nature, v. 417, p. 837–840, https://doi.org/10.1038/nature00799
Fukao, Y., Widiyantoro, S., and Obayashi, M., 2001, Stagnant slabs in the upper and lower mantle transition region: Reviews of Geophysics, v. 39, n. 3, p. 291–323, https://doi.org/10.1029/1999RG000068
GB/T14506.28-2010 (National Standard of P.R. China), 2011, Determination of 16 Major and Minor Elements Content (in Chinese).
Geng, Y. S., Liu, F. L., and Yang, C. H., 2006, Magmatic Event at the End of the Archean in Eastern Hebei Province and Its Geological Implication: Acta Geologica Sinica - English Edition, v. 80, n. 6, p. 819–833, https://doi.org/10.1111/j.1755-6724.2006.tb00305.x
Geng, Y. S., Du, L. L., and Ren, L. D., 2012, Growth and reworking of the early Precambrian continental crust in the North China Craton: Constraints from zircon Hf isotopes: Gondwana Research, v. 21, n. 2–3, p. 517–529, https://doi.org/10.1016/j.gr.2011.07.006
Goldsmith, J. R., 1980, The melting and breakdown reactions of anorthite at high pressures and temperatures: American Mineralogist, v. 65, n. 3–4, p. 272–284.
Guo, B. R., Liu, S. W., Santosh, M., and Wang, W., 2017, Neoarchean arc magmatism and crustal growth in the north-eastern North China Craton: Evidence from granitoid gneisses in the Southern Jilin Province: Precambrian Research, v. 303, p. 30–53, https://doi.org/10.1016/j.precamres.2016.12.009
Guo, J. H., Zhai, M. G., Zhang, Y. G., Li, Y. G., Yan, Y. H., and Zhang, W. H., 1993, Early Precambrian Manjinggou high-pressure granulites melange belt on the southern edge of the Huaian Complex, North China Craton: geological features, petrology and isotopic geochronology: Acta Petrologica Sinica, v. 9, p. 329341 (in Chinese).
Guo, J., Zhai, M., and Xu, R., 2001, Timing of the granulite facies metamorphism in the Sanggan area, North China craton: zircon U-Pb geochronology: Science in China Series D: Earth Sciences, v. 44, p. 1010–1018, https://doi.org/10.1007/BF02875394
Guo, J. H., O'Brien, P. J., and Zhai, M., 2002, High-pressure granulites in the Sanggan area, North China craton: metamorphic evolution, P-T paths and geotectonic significance: Journal of Metamorphic Geology, v. 20, n. 8, p. 741–756, https://doi.org/10.1046/j.1525-1314.2002.00401.x
Guo, J. H., Sun, M., Chen, F. K., and Zhai, M. G., 2005, Sm–Nd and SHRIMP U–Pb zircon geochronology of high-pressure granulites in the Sanggan area, North China Craton: timing of Paleoproterozoic continental collision: Journal of Asian Earth Sciences, v. 24, n. 5, p. 629–642, https://doi.org/10.1016/j.jseaes.2004.01.017
Han, B.-F., Xu, Z., Ren, R., Li, L.-L., Yang, J.-H., and Yang, Y.-H., 2012, Crustal growth and intracrustal recycling in the middle segment of the Trans-North China Orogen, North China Craton: a case study of the Fuping Complex: Geological Magazine, v. 149, n. 4, p. 729–742, https://doi.org/10.1017/S0016756811001014
Hawkesworth, C., Cawood, P., Kemp, T., Storey, C., and Dhuime, B., 2009, A Matter of Preservation: Science, v. 323, n. 5910, p. 49–50, https://doi.org/10.1126/science.1168549
Hawkesworth, C., Cawood, P. A., and Dhuime, B., 2019, Rates of generation and growth of the continental crust: Geoscience Frontiers, v. 10, n. 1, p. 165–173, https://doi.org/10.1016/j.gsf.2018.02.004

Hoffman, P. F., 1988, United Plates of America, The Birth of a Craton: Early Proterozoic Assembly and Growth of Laurentia: Annual Review of Earth and Planetary Sciences, v. 16, p. 543–603, https://doi.org/10.1146/annurev.ea.16.050188.002551

Hofmann, A. W., and Feigenson, M. D.., 1983, Case studies on the origin of basalt: Contributions to Mineralogy and Petrology, v. 84, n. 4, p. 382–389, https://doi.org/10.1007/BF01160289

Huang, X.-L., Niu, Y., Xu, Y.-G., Yang, Q.-J., and Zhong, J.-W., 2010, Geochemistry of TTG and TTG-like gneisses from Lushan-Taihua complex in the southern North China Craton: Implications for late Archean crustal accretion: Precambrian Research, v. 182, n. 1–2, p. 43–56, https://doi.org/10.1016/j.precamres.2010.06.020

Jahn, B.-m., and Zhang, Z. Q., 1984, Archean granulite gneisses from eastern Hebei Province, China: rare earth geochemistry and tectonic implications: Contributions to Mineralogy and Petrology, v. 85, p. 224–243, https://doi.org/10.1007/BF00378102

Jochum, K. P., and Nohl, U., 2008, Reference materials in geochemistry and environmental research and the GeoReM database: Chemical Geology, v. 253, n. 1–2, p. 50–53, https://doi.org/10.1016/j.chemgeo.2008.04.002

Kamber, B. S., Ewart, A., Collerson, K. D., Bruce, M. C., and McDonald, G. D., 2002, Fluid-mobile trace element constraints on the role of slab melting and implications for Archaean crustal growth models: Contributions to Mineralogy and Petrology, v. 144, p. 38–56, https://doi.org/10.1007/s00410-002-0374-5

Kay, S. M., Ramos, V. A., and Marquez, M., 1993, Evidence in Cerro Pampa Volcanic Rocks for Slab-Melting Prior to Ridge-Trench Collision in Southern South America: The Journal of Geology, v. 101, n. 6, p. 703–714, https://doi.org/10.1086/648269

Kleinhanns, I. C., Kramers, J. D., and Kamber, B. S., 2003, Importance of water for Archaean granitoid petrology: a comparative study of TTG and potassic granitoids from Barberton Mountain Land, South Africa: Contributions to Mineralogy and Petrology, v. 145, p. 377–389, https://doi.org/10.1007/s00410-003-0459-9

Klemme, S., Prowatke, S., Hametner, K., and Günther, D., 2005, Partitioning of trace elements between rutile and silicate melts: Implications for subduction zones: Geochimica et Cosmochimica Acta, v. 69, n. 9, p. 2361–2371, https://doi.org/10.1016/j.gca.2004.11.015

Kröner, A., and Layer, P. W., 1992, Crust Formation and Plate Motion in the Early Archean: Science, v. 256, n. 5062, p. 1405–1411, https://doi.org/10.1126/science.256.5062.1405

Kröner, A., Wilde, S. A., Li, J. H., and Wang, K. Y., 2005a, Age and evolution of a late Archean to Paleoproterozoic upper to lower crustal section in the Wutaishan/Hengshan/Fuping terrain of northern China: Journal of Asian Earth Sciences, v. 24, n. 5, p. 577–595, https://doi.org/10.1016/j.jseaes.2004.01.001

Kröner, A., Wilde, S. A., O'Brien, P. J., Li, J. H., Passchier, C. W., Walte, N. P., and Liu, D. Y., 2005b, Field relationships, geochemistry, zircon ages and evolution of a late Archaean to Palaeoproterozoic lower crustal section in the Hengshan Terrain of northern China: Acta Geologica Sinica, v. 79, p. 605-629

Kröner, A., Wilde, S. A., Zhao, G. C., O'Brien, P. J., Sun, M., Liu, D. Y., Wan, Y. S., Liu, S. W., and Guo, J. H., 2006, Zircon geochronology and metamorphic evolution of mafic dykes in the Hengshan Complex of northern China: Evidence for late Palaeoproterozoic extension and subsequent high-pressure metamorphism in the North China Craton: Precambrian Research, v. 146, n. 1–2, p. 45–67, https://doi.org/10.1016/j.precamres.2006.01.008

Kusky, T. M., Polat, A., Windley, B. F., Burke, K. C., Dewey, J. F., Kidd, W. S. F., Maruyama, S., Wang, J. P., Deng, H., Wang, Z. S., Wang, C., Fu, D., Li, X. W., and Peng, H. T., 2016, Insights into the tectonic evolution of the North China Craton through comparative tectonic analysis: A record of outward growth of Precambrian continents: Earth-Science Reviews, v. 162, p. 387–432, https://doi.org/10.1016/j.earscirev.2016.09.002

Li, J. H., Zhai, M. G., Qian, X. L., Guo, J. H., Wang, G. Y., Yan, Y. H., and Li, Y. G., 1998, The geological occurrence, regional tectonic setting and exhumation of late Archean high-pressure granulite within the high-grade metamorphic terrains, north to central portion of North China Craton: Acta Petrologica Sinica, v. 14, p. 176–189.

Li, S. Z., and Zhao, G. C., 2007, SHRIMP U–Pb zircon geochronology of the Liaoji granitoids: Constraints on the evolution of the Paleoproterozoic Jiao-Liao-Ji belt in the Eastern Block of the North China Craton: Precambrian Research, v. 158, n. 1–2, p. 1–16, https://doi.org/10.1016/j.precamres.2007.04.001

Li, S. Z., Zhao, G. C., Sun, M., Han, Z. Z., Hao, D. F., Luo, Y., and Xia, X. P., 2005, Deformation history of the Paleoproterozoic Liaohe assemblage in the eastern block of the North China Craton: Journal of Asian Earth Sciences, v. 24, n. 5, p. 659–674, https://doi.org/10.1016/j.jseaes.2003.11.008

Li , S. Z., Zhao, G. C., Wilde, S. A., Zhang, J., Sun, M., Zhang, G. W., and Dai, L. M., 2010, Deformation history of the Hengshan–Wutai–Fuping Complexes: Implications for the evolution of the Trans-North China Orogen: Gondwana Research, v. 18, n. 4, p. 611–631, https://doi.org/10.1016/j.gr.2010.03.003

Li, S. Z., Zhao, G. C., Santosh, M., Liu, X., and Dai, L. M., 2011a, Palaeoproterozoic tectonothermal evolution and deep crustal processes in the Jiao-Liao-Ji Belt, North China Craton: a review: Geological Journal, v. 46, n. 6, p. 525–543, https://doi.org/10.1002/gj.1282

Li, S. Z., Zhao, G. C., Santosh, M., Liu, X., Dai, L. M, Suo, Y. H., Song, M. C, and Wang, P. C., 2012, Paleoproterozoic structural evolution of the southern segment of the Jiao-Liao-Ji Belt, North China Craton: Precambrian Research, v. 200–203, p. 59–73, https://doi.org/10.1016/j.precamres.2012.01.007

Li, X. P., Yang, Z. Y., Zhao, G. C., Grapes, R., and Guo, J. H., 2011b, Geochronology of khondalite-series rocks of the Jining Complex: confirmation of depositional age and tectonometamorphic evolution of the North China craton: International Geology Review, v. 53, n. 10, p. 1194–1211., https://doi.org/10.1080/00206810903548984

Liu, C. H., Zhao, G. C., Liu, F. L., Sun, M., Zhang, J., and Yin, C. Q., 2012a, Zircons U-Pb and Lu-Hf isotopic and whole-rock geochemical constraints on the Gantaohe Group in the Zanhuang Complex: Implications for the tectonic evolution of the Trans-North China Orogen: Lithos, v. 146–147, p. 80–92, https://doi.org/10.1016/j.lithos.2012.04.033

Liu, C. H., Zhao, G. C., Sun, M., Zhang, J., and Yin, C. Q., 2012b, U–Pb geochronology and Hf isotope geochemistry of detrital zircons from the Zhongtiao Complex: Constraints on the tectonic evolution of the Trans-North China Orogen: Precambrian Research, v. 222–223, p. 159–172, https://doi.org/10.1016/j.precamres.2011.08.007

Liu, C. H., Zhao, G. C., Sun, M., Zhang, J., Yin, C. Q., and He, Y. H., 2012c, Detrital zircon U–Pb dating, Hf isotopes and whole-rock geochemistry from the Songshan Group in the Dengfeng Complex: Constraints on the tectonic evolution of the Trans-North China Orogen: Precambrian Research, v. 192–195, p. 1–15, https://doi.org/10.1016/j.precamres.2011.10.006

Liu, C. H., Liu, F. L., and Zhao, G. C., 2013a, Provenance and tectonic setting of the Jiehekou Group in the Lüliang complex: Constraints from zircon U-Pb age and Hf isotopic studies: Acta Petrologica Sinica, v. 29, p. 517–532.

Liu, D. Y., Page, R. W., Compston, W., and Wu, J. S., 1985, U-Pb zircon geochronology of late Archaean metamorphic rocks in the Taihangshan—Wutaishan area, North China: Precambrian Research, v. 27, n. 1–3, p. 85–109, https://doi.org/10.1016/0301-9268(85)90007-5

Liu, D. Y., Nutman, A. P., Compston, W., Wu, J. S., and Shen, Q. H., 1992, Remnants of ≥3800 Ma crust in the Chinese part of the Sino-Korean craton: Geology, v. 20, n. 4, p. 339–342, https://doi.org/10.1130/0091-7613(1992)020<0339:ROMCIT>2.3.CO;2

Liu, D. Y., Geng, Y. S., and Song, B., 1997, Late Archean Crustal Accretion and Reworking in Northwest Hebei Province: isochronology Evidence: Acta Geoscientia Sinica-Bulletin of the Chinese Academy of Geological Sciences, v. 18, p. 226–232.

Liu, D. Y., Wilde, S. A., Wan, Y. S., Wang, S. Y., Valley, J. W., Kita, N., Dong, C. Y., Xie, H. Q., Yang, C. X., Zhang, Y. X., and Gao, L Z., 2009a, Combined U–Pb, hafnium and oxygen isotope analysis of zircons from meta-igneous rocks in the southern North China Craton reveal multiple events in the Late Mesoarchean–Early Neoarchean: Chemical Geology, v. 261, n. 1–2, p. 140–154, https://doi.org/10.1016/j.chemgeo.2008.10.041

Liu, F., Guo, J. H., Lu, X. P., and Diwu, C. R., 2009b, Crustal growth at ~2.5 Ga in the North China Craton: evidence from whole-rock Nd and zircon Hf isotopes in the Huai'an gneiss terrane: Chinese Science Bulletin, v. 54, p. 4704–4713, https://doi.org/10.1007/s11434-009-0288-y

Liu, F., Guo, J.-H., Peng, P., and Qian, Q., 2012d, Zircon U–Pb ages and geochemistry of the Huai'an TTG gneisses terrane: Petrogenesis and implications for ~2.5Ga crustal growth in the North China Craton: Precambrian Research, v. 212–213, p. 225–244, https://doi.org/10.1016/j.precamres.2012.06.006

Liu, J. H., Liu, F. L., Ding, Z. J., Liu, C. H., Yang, H., Liu, P. H., Wang, F., and Meng, E., 2013b, The growth, reworking and metamorphism of early Precambrian crust in the Jiaobei terrane, the North China Craton: Constraints from U–Th–Pb and Lu–Hf isotopic systematics, and REE concentrations of zircon from Archean granitoid gneisses: Precambrian Research, v. 224, p. 287–303, https://doi.org/10.1016/j.precamres.2012.10.003

Liu, S. W., Pan, Y. M., Li, J. H., Li, Q. G., and Zhang, J., 2002, Geological and isotopic geochemical constraints on the evolution of the Fuping Complex, North China Craton: Precambrian Research, v. 117, n. 1–2, p. 41–56, https://doi.org/10.1016/S0301-9268(02)00063-3

Liu, S. W., Pan, Y. M, Xie, Q. L., Zhang, J., and Li, Q. G., 2004, Archean geodynamics in the Central Zone, North China Craton: constraints from geochemistry of two contrasting series of granitoids in the Fuping and Wutai complexes: Precambrian Research, v. 130, n. 1–4, p. 229–249, https://doi.org/10.1016/j.precamres.2003.12.001

Liu, S. W., Wei, T., Tian, W., LÜ, Y. J, LI, Q., Feng, Y. G., Park, K. H., and Song, Y. S., 2006, Geochemistry, Nd Isotopic Characteristics of Metamorphic Complexes in Northern Hebei: Implications for Crustal Accretion: Acta Geologica Sinica - English Edition, v. 80, p. 807–818, https://doi.org/10.1111/j.1755-6724.2006.tb00304.x

Liu, S. W., Zhang, J., Li, Q. G., Zhang, L. F., Wang, W., and Yang, P. T., 2012e, Geochemistry and U–Pb zircon ages of metamorphic volcanic rocks of the Paleoproterozoic Lüliang Complex and constraints on the evolution of the Trans-North China Orogen, North China Craton: Precambrian Research, v. 222–223, p. 173–190, https://doi.org/10.1016/j.precamres.2011.07.006

Lu, L., and Jin, S., 1993, P-T-t paths and tectonic history of an early Precambrian granulite facies terrane, Jining district, south-east Inner Mongolia, China: Journal of Metamorphic Geology, v. 11, n. 4, p. 483–498, https://doi.org/10.1111/j.1525-1314.1993.tb00166.x

Lu, L. Z., Xu, X. C., and Liu, F. L., 1996, Early Precambrian Khondalite Series in North China: Changchun, China, Changchun Publishing House, v. 276.

Luo, Y., Sun, M., Zhao, G. C., Li, S. Z., Xu, P., Ye, K., and Xia, X. P., 2004, LA-ICP-MS U–Pb zircon ages of the Liaohe Group in the Eastern Block of the North China Craton: constraints on the evolution of the Jiao-Liao-Ji Belt: Precambrian Research, v. 134, n. 3–4, p. 349–371, https://doi.org/10.1016/j.precamres.2004.07.002

Luo, Y., Sun, M., Zhao, G. C., Li, S. Z., Ayers, J. C., Xia, X. P., and Zhang, J. H., 2008, A comparison of U–Pb and Hf isotopic compositions of detrital zircons from the North and South Liaohe Groups: Constraints on the evolution of the Jiao-Liao-Ji Belt, North China Craton: Precambrian Research, v. 163, n. 3–4, p. 279–306, https://doi.org/10.1016/j.precamres.2008.01.002

Maniar, P. D., and Piccoli, P. M., 1989, Tectonic discrimination of granitoids: Geological Society of America Bulletin, v. 101, n. 5, p. 635–643, https://doi.org/10.1130/0016-7606(1989)101<0635:TDOG>2.3.CO;2

Martin, H., 1986, Effect of steeper Archean geothermal gradient on geochemistry of subduction-zone magmas: Geology, v. 14, n. 9, p. 753–756, https://doi.org/10.1130/0091-7613(1986)14<753:EOSAGG>2.0.CO;2

Martin, H., 1987, Petrogenesis of Archaean Trondhjemites, Tonalites, and Granodiorites from Eastern Finland: Major and Trace Element Geochemistry: Journal of Petrology, v. 28, n. 5, p. 921–953, https://doi.org/10.1093/petrology/28.5.921
Martin, H., 1999, Adakitic magmas: modern analogues of Archaean granitoids: Lithos, v. 46, n. 3, p. 411–429, https://doi.org/10.1016/S0024-4937(98)00076-0
Martin, H., and Moyen, J.-F., 2002, Secular changes in tonalite-trondhjemite-granodiorite composition as markers of the progressive cooling of Earth: Geology, v. 30, n. 4, p. 319, https://doi.org/10.1130/0091-7613(2002)030<0319:SCITTG>2.0.CO;2
Martin, H., Smithies, R. H., Rapp, R., Moyen, J.-F., and Champion, D., 2005, An overview of adakite, tonalite–trondhjemite–granodiorite (TTG), and sanukitoid: relationships and some implications for crustal evolution: Lithos, v. 79, n. 1–2, p. 1–24, https://doi.org/10.1016/j.lithos.2004.04.048
Maury, R. C., Sajona, F. G., Pubellier, M., Bellon, H., and Defant, M. J., 1996, Fusion de la croute oceanique dans les zones de subduction/collision recentes; l'exemple de Mindanao (Philippines): Bulletin de la Société Géologique de France, v. 167, n. 5, p. 579–595.
Moyen, J.-F., 2011, The composite Archaean grey gneisses: Petrological significance, and evidence for a non-unique tectonic setting for Archaean crustal growth: Lithos, v. 123, n. 1–4, p. 21–36, https://doi.org/10.1016/j.lithos.2010.09.015
Moyen, J.-F., and Martin, H., 2012, Forty years of TTG research: Lithos, v. 148, p. 312–336, https://doi.org/10.1016/j.lithos.2012.06.010
Moyen, J.-F., and Stevens, G., 2006, Experimental constraints on TTG petrogenesis: Implications for Archean geodynamics , in Benn, K., Mareschal, J.-C., and Condie, K., editors, Archean Geodynamics and Environments: American Geophysical Union, v. 164, p. 149–175, https://doi.org/10.1029/164GM11
Pearce, J. A., Harris, N. B. W., and Tindle, A. G., 1984, Trace Element Discrimination Diagrams for the Tectonic Interpretation of Granitic Rocks: Journal of Petrology, v. 25, n. 4, p. 956–983, https://doi.org/10.1093/petrology/25.4.956
Peccerillo, A., and Taylor, S. R., 1976, Geochemistry of eocene calc-alkaline volcanic rocks from the Kastamonu area, Northern Turkey: Contributions to Mineralogy and Petrology, v. 58, p. 63–81, https://doi.org/10.1007/BF00384745
Petford, N., and Atherton, M., 1996, Na-rich Partial Melts from Newly Underplated Basaltic Crust: the Cordillera Blanca Batholith, Peru: Journal of Petrology, v. 37, n. 6, p. 1491–1521, https://doi.org/10.1093/petrology/37.6.1491
Prouteau, G., Scaillet, B., Pichavant, M., and Maury, R., 2001, Evidence for mantle metasomatism by hydrous silicic melts derived from subducted oceanic crust: Nature, v. 410, p. 197–200, https://doi.org/10.1038/35065583
Rapp, R. P., and Watson, E. B., 1995, Dehydration Melting of Metabasalt at 8-32 kbar: Implications for Continental Growth and Crust-Mantle Recycling: Journal of Petrology, v. 36, n. 4, p. 891–931, https://doi.org/10.1093/petrology/36.4.891
Rapp, R. P., Shimizu, N., Norman, M. D., and Applegate, G. S., 1999, Reaction between slab-derived melts and peridotite in the mantle wedge: experimental constraints at 3.8 GPa: Chemical Geology, v. 160, n. 4, p. 335–356, https://doi.org/10.1016/S0009-2541(99)00106-0
Rapp, R. P., Norman, M. D., Laporte, D., Yaxley, G. M., Martin, H., and Foley, S. F., 2010, Continent Formation in the Archean and Chemical Evolution of the Cratonic Lithosphere: Melt-Rock Reaction Experiments at 3-4 GPa and Petrogenesis of Archean Mg-Diorites (Sanukitoids): Journal of Petrology, v. 51, n. 6, p. 1237–1266, https://doi.org/10.1093/petrology/egq017
Rollinson, H., 2010, Coupled evolution of Archean continental crust and subcontinental lithospheric mantle: Geology, v. 38, n. 12, p. 1083–1086, https://doi.org/10.1130/G31159.1
Rollinson, H. R., 2014, Using Geochemical Data: New York, Routledge, 384 p. https://doi.org/10.4324/9781315845548
Romanowicz, B., and Gung, Y. C., 2002, Superplumes from the Core-Mantle Boundary to the Lithosphere: Implications for Heat Flux: Science, v. 296, n. 5567, p. 513–516, https://doi.org/10.1126/science.1069404
Rushmer, T., 1991, Partial melting of two amphibolites: contrasting experimental results under fluid-absent conditions: Contributions to Mineralogy and Petrology, v. 107, p. 41–59, https://doi.org/10.1007/BF00311184
Santosh, M., 2010a, Assembling North China Craton within the Columbia supercontinent: The role of double-sided subduction: Precambrian Research, v. 178, n. 1–4, p. 149–167, https://doi.org/10.1016/j.precamres.2010.02.003
Santosh, M., 2010b, A synopsis of recent conceptual models on supercontinent tectonics in relation to mantle dynamics, life evolution and surface environment: Journal of Geodynamics, v. 50, n. 3–4, p. 116–133, https://doi.org/10.1016/j.jog.2010.04.002
Schiano, P., Monzier, M., Eissen, J.-P., Martin, H., and Koga, K. T., 2010, Simple mixing as the major control of the evolution of volcanic suites in the Ecuadorian Andes: Contributions to Mineralogy and Petrology, v. 160, p. 297–312, https://doi.org/10.1007/s00410-009-0478-2
Schmidt, M. W., Dardon, A., Chazot, G., and Vannucci, R., 2004, The dependence of Nb and Ta rutile–melt partitioning on melt composition and Nb/Ta fractionation during subduction processes: Earth and Planetary Science Letters, v. 226, n. 3–4, p. 415–432, https://doi.org/10.1016/j.epsl.2004.08.010
Shan, H. X., Zhai, M. G., and Dey, S., 2016, Petrogenesis of Two Types of Archean TTGs in the North China Craton: A Case Study of Intercalated TTGs in Lushan and Non-intercalated TTGs in Hengshan: Acta Geologica Sinica-English Edition, v. 90, n. 6, p. 2049–2065, https://doi.org/10.1111/1755-6724.13021
Smithies, R. H., 2000, The Archaean tonalite–trondhjemite–granodiorite (TTG) series is not an analogue of Cenozoic adakite: Earth and Planetary Science Letters, v. 182, n. 1, p. 115–125, https://doi.org/10.1016/S0012-821X(00)00236-3

Smithies, R. H., and Champion, D. C., 2000, The Archaean High-Mg Diorite Suite: Links to Tonalite-Trondhjemite-Granodiorite Magmatism and Implications for Early Archaean Crustal Growth: Journal of Petrology, v. 41, n.12, p. 1653–1671, https://doi.org/10.1093/petrology/41.12.1653

Song, B., Nutman, A. P., Liu, D. Y., and Wu, J. S., 1996, 3800 to 2500 Ma crustal evolution in the Anshan area of Liaoning Province, northeastern China: Precambrian Research, v. 78, n. 1–3, p. 79–94, https://doi.org/10.1016/0301-9268(95)00070-4

Springer, W., and Seck, H. A., 1997, Partial fusion of basic granulites at 5 to 15 kbar: implications for the origin of TTG magmas: Contributions to Mineralogy and Petrology, v. 127, p. 30–45, https://doi.org/10.1007/s004100050263

Stern, C. R., and Kilian, R., 1996, Role of the subducted slab, mantle wedge and continental crust in the generation of adakites from the Andean Austral Volcanic Zone: Contributions to Mineralogy and Petrology, v. 123, p. 263–281, https://doi.org/10.1007/s004100050155

Su, Y. P., Zheng, J. P., Griffin, W. L., Zhao, J. H., Li, Y. L., Wei, Y., and Huang, Y., 2014, Zircon U–Pb ages and Hf isotope of gneissic rocks from the Huai'an Complex: Implications for crustal accretion and tectonic evolution in the northern margin of the North China Craton: Precambrian Research, v. 255, Part 1, p. 335–354, https://doi.org/10.1016/j.precamres.2014.10.007

Sun, M., Armstrong, R. L., and Lambert, R. S. J, 1992, Petrochemistry and Sr, Pb, and Nd isotopic geochemistry of early precambrian rocks, Wutaishan and Taihangshan areas, China: Precambrian Research, v. 56, n. 1–2, p. 1–31, https://doi.org/10.1016/0301-9268(92)90081-X

Sun, S. -s., and McDonough, W. F., 1989, Chemical and isotopic systematics of oceanic basalts: implications for mantle composition and processes: Geological Society, London, Special Publications, v. 42, p. 313–345, https://doi.org/10.1144/GSL.SP.1989.042.01.19

Tam, P. Y., Zhao, G. C., Liu, F. L., Zhou, X. W., Sun, M., and Li, S. Z., 2011, Timing of metamorphism in the Paleoproterozoic Jiao-Liao-Ji Belt: New SHRIMP U–Pb zircon dating of granulites, gneisses and marbles of the Jiaobei massif in the North China Craton: Gondwana Research, v. 19, n. 1, p. 150–162, https://doi.org/10.1016/j.gr.2010.05.007

Tam, P. Y., Zhao, G. C., Sun, M., Li, S. Z., Iizuka, Y., Ma, G. S.-K. i., Yin, C. Q., He, Y. H., and Wu, M. L., 2012a, Metamorphic P–T path and tectonic implications of medium-pressure pelitic granulites from the Jiaobei massif in the Jiao-Liao-Ji Belt, North China Craton: Precambrian Research, v. 220–221, p. 177–191, https://doi.org/10.1016/j.precamres.2012.08.008

Tam, P. Y., Zhao, G. C., Sun, M., Li, S. Z., Wu, M. L., and Yin, C. Q., 2012b, Petrology and metamorphic P–T path of high-pressure mafic granulites from the Jiaobei massif in the Jiao-Liao-Ji Belt, North China Craton: Lithos, v. 155, p. 94–109, https://doi.org/10.1016/j.lithos.2012.08.018

Tam, P. Y., Zhao, G. C, Zhou, X. W., Sun, M., Guo, J. H., Li, S. Z., Yin, C. Q., Wu, M. L., and He, Y. H., 2012c, Metamorphic P–T path and implications of high-pressure pelitic granulites from the Jiaobei massif in the Jiao-Liao-Ji Belt, North China Craton: Gondwana Research, v. 22, n. 1, p. 104–117, https://doi.org/10.1016/j.gr.2011.09.006

Tiepolo, M., Vannucci, R., Oberti, R., Foley, S., Bottazzi, P., and Zanetti, A., 2000, Nb and Ta incorporation and fractionation in titanian pargasite and kaersutite: crystal–chemical constraints and implications for natural systems: Earth and Planetary Science Letters, v. 176, n. 2, p. 185–201, https://doi.org/10.1016/S0012-821X(00)00004-2

Trap, P., Faure, M., Lin, W., Le Breton, N., and Monié, P., 2012, Paleoproterozoic tectonic evolution of the Trans-North China Orogen: Toward a comprehensive model: Precambrian Research, v. 222–223, p. 191–211, https://doi.org/10.1016/j.precamres.2011.09.008

Treuil M, J. J.-L, 1975, Utilisation des elements hygromagmatophiles pour la simplification de la mode'lisation quantitative des processus magmatiques: exemples de l'Afar et de la dorsale me'dio-atlantique: Società Italiana di Mineralogia e Petrologia, v. 31, p. 125–174.

Wan, Y. S., Liu, D. Y., Song, B., Wu, J. S., Yang, C. H., Zhang, Z. Q., and Geng, Y. S., 2005, Geochemical and Nd isotopic compositions of 3.8Ga meta-quartz dioritic and trondhjemitic rocks from the Anshan area and their geological significance: Journal of Asian Earth Sciences, v. 24, n. 5, p. 563–575, https://doi.org/10.1016/j.jseaes.2004.02.009

Wang, F., Li, X.-P., Chu, H., and Zhao, G., 2011, Petrology and metamorphism of khondalites from the Jining complex, North China craton: International Geology Review, v. 53, n. 1, p. 212–229, https://doi.org/10.1080/00206810903028144

Wang, W., Liu, S., Santosh, M., Wang, G., Bai, X., and Guo, R., 2015, Neoarchean intra-oceanic arc system in the Western Liaoning Province: Implications for Early Precambrian crustal evolution in the Eastern Block of the North China Craton: Earth-Science Reviews, v. 150, p. 329–364, https://doi.org/10.1016/j.earscirev.2015.08.002

Wang, W., Cawood, P. A., Liu, S., Guo, R., Bai, X., and Wang, K., 2017, Cyclic formation and stabilization of Archean lithosphere by accretionary orogenesis: Constraints from TTG and potassic granitoids, North China Craton: Tectonics, v. 36, p. 1724–1742, https://doi.org/10.1002/2017TC004600

Whalen, J. B., Percival, J. A., McNicoll, V. J., and Longstaffe, F. J., 2002, A mainly crustal origin for tonalitic granitoid rocks, Superior Province, Canada: implications for late Archean tectonomagmatic processes: Journal of Petrology, v. 43, n. 8, p. 1551–1570, https://doi.org/10.1093/petrology/43.8.1551

Wilde, S. A., and Zhao, G. C., 2005, Archean to Paleoproterozoic evolution of the North China Craton: Journal of Asian Earth Sciences, v. 24, n. 5, p. 519–522, https://doi.org/10.1016/j.jseaes.2004.06.004

Wilde, S. A., Zhao, G. C., and Sun, M., 2002, Development of the North China Craton During the Late Archaean and its Final Amalgamation at 1.8 Ga: Some Speculations on its Position Within a Global Palaeoproterozoic Supercontinent: Gondwana Research, v. 5, n. 1, p. 85–94, https://doi.org/10.1016/S1342-937X(05)70892-3

Woodhead, J. D., Hergt, J. M., Davidson, J. P., and Eggins, S. M., 2001, Hafnium isotope evidence for 'conservative' element mobility during subduction zone processes: Earth and Planetary Science Letters, v. 192, n. 3, p. 331–346, https://doi.org/10.1016/S0012-821X(01)00453-8

Wu, F. Y., Zhao, G. C., Wilde, S. A., and Sun, D. Y., 2005, Nd isotopic constraints on crustal formation in the North China Craton: Journal of Asian Earth Sciences, v. 24, n. 5, p. 523–545, https://doi.org/10.1016/j.jseaes.2003.10.011

Wu, J.-L., Zhang, H.-F., Zhai, M.-G., Guo, J.-H., Liu, L., Yang, W.-Q., Wang, H.-Z., Zhao, L., Jia, X.-L., and Wang, W., 2016, Discovery of pelitic high-pressure granulite from Manjinggou of the Huai'an Complex, North China Craton: Metamorphic P–T evolution and geological implications: Precambrian Research, v. 278, p. 323–336, https://doi.org/10.1016/j.precamres.2016.03.001

Wu, J. L., Zhang, H. F., Zhai, M. G., Zhang, H., Wang, H. Z., Li, R., Hu, B., and Zhang, H. D., 2019, Shared metamorphic histories of various Palaeoproterozoic granulites from Datong–Huai'an area, North China Craton (NCC): constraints from zircon U–Pb ages and petrology: International Geology Review, v. 61, n. 6, p. 694–719, https://doi.org/10.1080/00206814.2018.1449022

Wu, M. L., Zhao, G. C., Sun, M., Li, S. Z., Bao, Z. A., Tam, P. Y., Eizenhöefer, P. R., and He, Y. H., 2014, Zircon U–Pb geochronology and Hf isotopes of major lithologies from the Jiaodong Terrane: Implications for the crustal evolution of the Eastern Block of the North China Craton: Lithos, v. 190–191, p. 71–84, https://doi.org/10.1016/j.lithos.2013.12.004

Xia, X. P., Sun, M., Zhao, G. C., and Luo, Y., 2006a, LA-ICP-MS U-Pb geochronology of detrital zircons from the Jining Complex, North China Craton and its tectonic significance: Precambrian Research, v. 144, n. 3–4, p. 199–212, https://doi.org/10.1016/j.precamres.2005.11.004

Xia, X. P., Sun, M., Zhao, G. C., Wu, F. Y., Xu, P., Zhang, J. H., and Luo, Y., 2006b, U–Pb and Hf isotopic study of detrital zircons from the Wulashan khondalites: Constraints on the evolution of the Ordos Terrane, Western Block of the North China Craton: Earth and Planetary Science Letters, v. 241, n. 3–4, p. 581–593, https://doi.org/10.1016/j.epsl.2005.11.024

Xiao, L.-L., Wu, C.-M., Zhao, G.-C., Guo, J.-H., and Ren, L.-D., 2011, Metamorphic P–T paths of the Zanhuang amphibolites and metapelites: constraints on the tectonic evolution of the Paleoproterozoic Trans-North China Orogen: International Journal of Earth Sciences, v. 100, p. 717–739, https://doi.org/10.1007/s00531-010-0522-5

Xiong, X.-L., 2006, Trace element evidence for growth of early continental crust by melting of rutile-bearing hydrous eclogite: Geology, v. 34, n. 11, p. 945–948, https://doi.org/10.1130/G22711A.1

Xiong, X. L., Adam, J., and Green, T. H., 2005, Rutile stability and rutile/melt HFSE partitioning during partial melting of hydrous basalt: Implications for TTG genesis: Chemical Geology, v. 218, n. 3–4, p. 339–359, https://doi.org/10.1016/j.chemgeo.2005.01.014

Xiong, X. L., Keppler, H., Audétat, A., Gudfinnsson, G., Sun, W. D., Song, M. S., Xiao, W. S., and Yuan, L., 2009, Experimental constraints on rutile saturation during partial melting of metabasalt at the amphibolite to eclogite transition, with applications to TTG genesis: American Mineralogist, v. 94, n. 8–9, p. 1175–1186, https://doi.org/10.2138/am.2009.3158

Yin, C. Q., Zhao, G. C., Sun, M., Xia, X. P., Wei, C. J., Zhou, X. W., and Leung, W. H., 2009, LA-ICP-MS U–Pb zircon ages of the Qianlishan Complex: Constrains on the evolution of the Khondalite Belt in the Western Block of the North China Craton: Precambrian Research, v. 174, n. 1–2. 78–94, https://doi.org/10.1016/j.precamres.2009.06.008

Yin, C. Q., Zhao, G. C., Guo, J. H., Sun, M., Xia, X. P., Zhou, X. W., and Liu, C. H., 2011, U–Pb and Hf isotopic study of zircons of the Helanshan Complex: Constrains on the evolution of the Khondalite Belt in the Western Block of the North China Craton: Lithos, v. 122, n. 1–2, p. 25–38, https://doi.org/10.1016/j.lithos.2010.11.010

Yin, C. Q., Zhao, G. C., Wei, C. J., Sun, M., Guo, J. H., and Zhou, X. W., 2014, Metamorphism and partial melting of high-pressure pelitic granulites from the Qianlishan Complex: Constraints on the tectonic evolution of the Khondalite Belt in the North China Craton: Precambrian Research, v. 242, p. 172–186, https://doi.org/10.1016/j.precamres.2013.12.025

Yin, C. Q., Zhao, G. C., and Sun, M., 2015, High-pressure pelitic granulites from the Helanshan Complex in the Khondalite Belt, North China Craton: Metamorphic P-t path and tectonic implications: American Journal of Science, v. 315, n. 9, p. 846–879, https://doi.org/10.2475/09.2015.03

Zhai, M. G., 2012, Evolution of the North China Craton and early plate tectonics: Acta Geologica Sinica, v. 86, p. 1335–1349.

Zhai, M. G., 2014, Multi-stage crustal growth and cratonization of the North China Craton: Geoscience Frontiers, v. 5, n. 4, p. 457–469, https://doi.org/10.1016/j.gsf.2014.01.003

Zhai, M. G., editor, 2015, Precambrian Geology of China: Berlin, Heidelberg, Germany, Springer, 390 p., https://doi.org/10.1007/978-3-662-47885-1

Zhai, M.-G., and Santosh, M., 2011, The early Precambrian odyssey of the North China Craton: A synoptic overview: Gondwana Research, v. 20, n. 1, p. 6–25, https://doi.org/10.1016/j.gr.2011.02.005

Zhai, M. G., Guo, J. H., Yan, Y. H., Han, X. L., and Li, Y. G., 1992, Discovery and preliminary study of the Archean high-pressure granulites in the North China: Science in China, v. 12, p. 1325–1330.

Zhai, M. G., Guo, J. H., Yan, Y. H., Li, Y. G., and Han, X. L., 1993, Discovery of high-pressure basic granulite terrain in north China Archaean Craton and preliminary study: Science in China, Ser. B, p. 13.

Zhai, M. G., Guo, J. H., Li, H. H., Yan, Y. H., and Li, Y. G., 1995, Discovery of retrograded eclogites in the Archaean North China Craton: Chinese Science Bulletin, v. 40, p. 1590–1594.

Zhai, M. G., Santosh, M., and Zhang, L. C., 2011, Precambrian geology and tectonic evolution of the North China Craton: Gondwana Research, v. 20, n. 1, p. 1–5, https://doi.org/10.1016/j.gr.2011.04.004

Zhang, H.-F., Zhai, M.-G., Santosh, M., and Li, S.-R., 2012a, Low-Al and high-Al trondhjemites in the Huai'an Complex, North China Craton: Geochemistry, zircon U–Pb and Hf isotopes, and implications

for Neoarchean crustal growth and remelting: Journal of Asian Earth Sciences, v. 49, p. 203–213, https://doi.org/10.1016/j.jseaes.2011.11.004
Zhang, H. F., Wang, H. Z., Dou, J. Z., and Zhang, S. Y., 2015, Geochemistry and genesis of the Late Archean Low-Al and High-Al TTGs from the Huai'an terrane, North China Craton: Acta Petrologica Sinica, v. 31, p. 1518–1534.
Zhang, J., Dirks, P. H. G. M., and Passchier, C. W., 1994, Extensional collapse and uplift in a polymetamorphic granulite terrain in the Archaean and Palaeoproterozoic of north China: Precambrian Research, v. 67, n. 1–2, p. 37–57, https://doi.org/10.1016/0301-9268(94)90004-3
Zhang, J., Zhao, G. C., Sun, M., Wilde, S. A., Li, S., and Liu, S. W., 2006, High-pressure mafic granulites in the Trans-North China Orogen: Tectonic significance and age: Gondwana Research, v. 9, n. 3, p. 349–362, https://doi.org/10.1016/j.gr.2005.10.005
Zhang, J., Zhao, G. C., Li, S. Z., Sun, M., Liu, S. W., Wilde, S. A., Kröner, A., and Yin, C. Q., 2007, Deformation history of the Hengshan Complex: Implications for the tectonic evolution of the Trans-North China Orogen: Journal of Structural Geology, v. 29, n. 6, p. 933–949, https://doi.org/10.1016/j.jsg.2007.02.013
Zhang, J., Zhao, G. C., Li, S. Z., Sun, M., Wilde, S. A., Liu, S. W., and Yin, C. Q., 2009, Polyphase deformation of the Fuping Complex, Trans-North China Orogen: Structures, SHRIMP U–Pb zircon ages and tectonic implications: Journal of Structural Geology, v. 31, n. 2, p. 177–193, https://doi.org/10.1016/j.jsg.2008.11.008
Zhang, J., Zhao, G. C., Li, S. Z., Sun, M., Chan, L. S., Shen, W. L., and Liu, S. W., 2012b, Structural pattern of the Wutai Complex and its constraints on the tectonic framework of the Trans-North China Orogen: Precambrian Research, v. 222–223, p. 212–229, https://doi.org/10.1016/j.precamres.2011.08.009
Zhao, D. Y., Sun, M., and Ding, A. Y., 2020, Zircon U-Pb ages and Hf isotopes of the Huai'an gneisses from the Tianzhen-Xinpingbu area: Implications for the tectonic evolution of the Trans-North China Orogen: Precambrian Research, v. 337, p. 105530, https://doi.org/10.1016/j.precamres.2019.105530
Zhao, G. C., 2001, Palaeoproterozoic assembly of the North China craton: Geological Magazine, v. 138, n. 1, p. 87–91, https://doi.org/10.1017/S0016756801005040
Zhao, G. C., 2009, Metamorphic evolution of major tectonic units in the basement of the North China Craton: key issues and discussion: Acta Petrologica Sinica, v. 25, p. 1772–1292.
Zhao, G. C., 2014, Tectonic Subdivision of the North China Craton, in Precambrian Evolution of the North China Craton: Amsterdam, the Netherlands, Elsevier, p. 1–14, https://doi.org/10.1016/B978-0-12-407227-5.00001-8
Zhao, G. C., and Cawood, P. A., 2012, Precambrian geology of China: Precambrian Research, v. 222–223, p. 13–54, https://doi.org/10.1016/j.precamres.2012.09.017
Zhao, G. C., and Zhai, M. G., 2013, Lithotectonic elements of Precambrian basement in the North China Craton: Review and tectonic implications: Gondwana Research, v. 23, n. 4, p. 1207–1240, https://doi.org/10.1016/j.gr.2012.08.016
Zhao, G. C., Wilde, S. A., Cawood, P. A., and Lu, L. Z., 1998, Thermal Evolution of Archean Basement Rocks from the Eastern Part of the North China Craton and Its Bearing on Tectonic Setting: International Geology Review, v. 40, n. 8, p. 706–721, https://doi.org/10.1080/00206819809465233
Zhao, G. C., Cawood, P. A., Wilde, S. A., Sun, M., and Lu, L. Z., 2000, Metamorphism of basement rocks in the Central Zone of the North China Craton: implications for Paleoproterozoic tectonic evolution: Precambrian Research, v. 103, n. 1–2, p. 55–88, https://doi.org/10.1016/S0301-9268(00)00076-0
Zhao, G. C., Cawood, P. A., Wilde, S., and Lu, L. Z., 2001a, High-pressure granulites (Retrograded Eclogites) from the Hengshan Complex, North China Craton: Petrology and tectonic implications: Journal of Petrology, v. 42, n. 6, p. 1141–1170. https://doi.org/10.1093/petrology/42.6.1141
Zhao, G. C., Wilde, S. A., Cawood, P. A., and Sun, M., 2001b, Archean blocks and their boundaries in the North China Craton: lithological, geochemical, structural and P-T path constraints and tectonic evolution: Precambrian Research, v. 107, n. 1–2, p. 45–73, https://doi.org/10.1016/S0301-9268(00)00154-6
Zhao, G. C., Cawood, P. A., Wilde, S. A., and Sun, M., 2002a, Review of global 2.1–1.8 Ga orogens: implications for a pre-Rodinia supercontinent: Earth-Science Reviews, v. 59, n. 1–4, p. 125–162, https://doi.org/10.1016/S0012-8252(02)00073-9
Zhao, G. C., Wilde, S. A., Cawood, P. A., and Sun, M., 2002b, SHRIMP U-Pb zircon ages of the Fuping Complex: implications for late Archean to Paleoproterozoic accretion and assembly of the North China Craton: American Journal of Science, v. 302, n. 3, p. 191–226, https://doi.org/10.2475/ajs.302.3.191
Zhao, G. C., Sun, M., and Wilde, S. A., 2003, Major tectonic units of the North China Craton and their Paleoproterozoic assembly: Science in China, Series D: Earth Sciences, v. 46, n. 1, p. 23–38. 10.1360/03yd9003
Zhao, G. C., Sun, M., Wilde, S. A., and Li, S. Z., 2005, Late Archean to Paleoproterozoic evolution of the North China Craton: key issues revisited: Precambrian Research, v. 136, n. 2, p. 177–202, https://doi.org/10.1016/j.precamres.2004.10.002
Zhao, G. C., Sun, M., Wilde, S. A., Li, S. Z., Liu, S. W., and Zhang, J., 2006, Composite nature of the North China Granulite-Facies Belt: Tectonothermal and geochronological constraints: Gondwana Research, v. 9, n. 3, p. 337–348, https://doi.org/10.1016/j.gr.2005.10.004
Zhao, G. C., Kröner, A., Wilde, S. A., Sun, M., Li, S. Z., Li, X. P., Zhang, J., Xia, X. P., and He, Y. H., 2007, Lithotectonic elements and geological events in the Hengshan-Wutai-Fuping belt: a synthesis and implications for the evolution of the Trans-North China Orogen: Geological Magazine, v. 144, n. 5, p. 753–775, https://doi.org/10.1017/S0016756807003561
Zhao, G. C., Wilde, S. A., Sun, M., Guo, J. H., Kröner, A., Li, S. Z., Li, X. P., and Zhang, J., 2008a, SHRIMP U-Pb zircon geochronology of the Huai'an Complex: constraints on late Archean to Paleoproterozoic

magmatic and metamorphic events in the Trans-North China Orogen: American Journal of Science, v. 308, n. 3, p. 270–303, https://doi.org/10.2475/03.2008.04

Zhao, G. C., Wilde, S. A., Sun, M., Li, S. Z., Li, X. P., and Zhang, J., 2008b, SHRIMP U-Pb zircon ages of granitoid rocks in the Lüliang Complex: Implications for the accretion and evolution of the Trans-North China Orogen: Precambrian Research, v. 160, n. 3–4, p. 213–226, https://doi.org/10.1016/j.precamres.2007.07.004

Zhao, G. C., Cawood, P. A., Li, S. Z., Wilde, S. A., Sun, M., Zhang, J., He, Y. H., and Yin, C. Q., 2012, Amalgamation of the North China Craton: Key issues and discussion: Precambrian Research, v. 222–223, p. 55–76, https://doi.org/10.1016/j.precamres.2012.09.016

Zhao, G. C., Wilde, S. A., Guo, J. H., Cawood, P. A., Sun, M., and Li, X. P., 2010, Single zircon grains record two Paleoproterozoic collisional events in the North China Craton: Precambrian Research, v. 177, n. 3–4, p. 266–276, https://doi.org/10.1016/j.precamres.2009.12.007

Zhou, X. W., Zhao, G. C., Wei, C. J., Geng, Y. S., and Sun, M., 2008, Metamorphic evolution and Th-U-Pb zircon and monazite geochronology of high-pressure pelitic granulites in the Jiaobei massif of the North China Craton: American Journal of Science, v. 308, p. 328–350, https://doi.org/10.2475/03.2008.06

Zhou, X. W., Zhao, G. C., and Geng, Y. S., 2010, Helanshan high-pressure pelitic granulites: petrological evidence for collision event in the Western Block of the North China Craton: Acta Petrologica Sinica.

Zhou, Y. Y., Zhao, T. P., Xue, L. W., Wang, S. Y., and Gao, J. F., 2009, Petrological, geochemical and chronological constraints for the origin and geological significance of Neoarchean TTG gneiss in the Songshan area, North China Craton: Acta Petrologica Sinica, v. 25, p. 331–347.